The plasmablast response to SARS-CoV-2 mRNA vaccination is dominated by non-neutralizing antibodies that target both the NTD and the RBD

Fatima Amanat[1,2], Mahima Thapa[3], Tinting Lei[3], Shaza M. Sayed Ahmed[3], Daniel C. Adelsberg[1], Juan Manuel Carreno[1], Shirin Strohmeier[1], Aaron J. Schmitz[3], Sarah Zafar[1], Julian Q Zhou[4], Willemijn Rijnink[1], Hala Alshammary[1], Nicholas Borcherding[3], Ana Gonzalez Reiche[5], Komal Srivastava, Emilia Mia Sordillo[6], Harm van Bakel[5,7], The Personalized Virology Initiative[#], Jackson S. Turner[3], Goran Bajic[1], Viviana Simon[9,10], Ali H. Ellebedy[3,11], Florian Krammer[1]

Affiliations

[1]Department of Microbiology, Icahn School of Medicine at Mount Sinai, New York, NY 10029.
[2]Graduate School of Biomedical Sciences, Icahn School of Medicine at Mount Sinai, New York, NY 10029.
[3]Department of Pathology & Immunology, Washington University School of Medicine, St. Louis, MO, 63110
[4]AbCellera Biologics Inc., Vancouver, BC V5Y 0A1, Canada
[5]Department of Genetics and Genomic Sciences, Icahn School of Medicine at Mount Sinai, New York, NY 10029
[6]Department of Pathology, Molecular and Cell Based Medicine, Icahn School of Medicine at Mount Sinai, New York, NY 10029
[7]Icahn Institute for Data Science and Genomic Technology, Icahn School of Medicine at Mount Sinai, New York, NY 10029, USA
[8]Division of Infectious Diseases, Department of Medicine, Icahn School of Medicine at Mount Sinai, New York, NY 10029.
[9]The Global Health and Emerging Pathogens Institute, Icahn School of Medicine at Mount Sinai, New York, NY 10029, USA.
[10]Andrew M. and Jane M. Bursky Center for Human Immunology and Immunotherapy Programs, Washington University School of Medicine, Saint Louis, MO 63110

[#]Personalized Virology Initiative (PVI) Study group/Consortium (in alphabetical order): Dr. Bulbul Ahmed, Dr. Deena Altman, Angela Amoako, Mahmoud Awawda, Katherine Beach, Carolina Bermúdez-González, Rachel Chernet, Lily Eaker, Shelcie Fabre, Emily. D. Ferreri, Daniel Floda, Charles Gleason, Dr. Giulio Kleiner, Dr. Denise Jurczyszak, Julia Matthews, Wanni Mendez, Dr. Lubbertus CF Mulder, Jose Polanco, Kayla Russo, Ashley Salimbangon, Dr. Miti Saksena, Amber S. Shin , Levy Sominsky, Sayahi Suthakaran, Dr. Ania Wajnberg

Corresponding authors

Goran Bajic, goran.bajic@mssm.edu

Viviana Simon, viviana.simon@mssm.edu

Ali H. Ellebedy, ellebedy@wustl.edu

Florian Krammer, florian.krammer@mssm.edu

Summary

In this study we profiled vaccine-induced polyclonal antibodies as well as plasmablast derived mAbs from subjects who received SARS-CoV-2 spike mRNA vaccine. Polyclonal antibody responses in vaccinees were robust and comparable to or exceeded those seen after natural infection. However, that the ratio of binding to neutralizing antibodies after vaccination was greater than that after natural infection and, at the monoclonal level, we found that the majority of vaccine-induced antibodies did not have neutralizing activity. We also found a co-dominance of mAbs targeting the NTD and RBD of SARS-CoV-2 spike and an original antigenic-sin like backboost to seasonal human coronaviruses OC43 and HKU1 spike proteins. Neutralizing activity of NTD mAbs but not RBD mAbs against a clinical viral isolate carrying E484K as well as extensive changes in the NTD was abolished, suggesting that a proportion of vaccine induced RBD binding antibodies may provide substantial protection against viral variants carrying E484K.

63 **Introduction**

64 Understanding of the innate and adaptive immune response to severe acute respiratory
65 syndrome coronavirus 2 (SARS-CoV-2) has progressed rapidly since the beginning of the coronavirus
66 disease 2019 (COVID-19) pandemic. Polyclonal antibody responses against the spike protein of the virus
67 in serum, and to a lesser degree also at mucosal surfaces, have been well characterized with respect to
68 their kinetics, binding capacity and functionality (Grandjean et al., 2020; Isho et al., 2020; Iyer et al., 2020;
69 Ripperger et al., 2020; Seow et al., 2020; Wajnberg et al., 2020). Similarly, much encouraging data has
70 been published about both the plasmablast response and the memory B-cell response induced by SARS-
71 CoV-2 infection (Dan et al., 2021; Gaebler et al., 2020; Guthmiller et al., 2021; Robbiani et al., 2020; Rodda
72 et al., 2021; Wilson et al., 2020). The immune responses to SARS-CoV-2 vaccination, including to mRNA-
73 based vaccines, are less well studied since these vaccines have only become available in the last months
74 of 2020 (Baden et al., 2020; Polack et al., 2020). However, understanding vaccine-induced immunity is of
75 high importance given the goal to achieve immunity for most people through vaccination, rather than as
76 a consequence of infection.

77 The receptor binding domain (RBD) of the SARS-CoV-2 spike is an important target for serological
78 and B-cell studies because it directly interacts with the cellular receptor angiotensin converting enzyme 2
79 (ACE2) mediating host cell entry (Letko et al., 2020; Wrapp et al., 2020). Antibodies binding to the RBD
80 can potently block attachment of the virus to ACE2 and thereby neutralize the virus (Barnes et al., 2020).
81 As a consequence, RBD-based vaccines are in development in addition to full length spike-based vaccines
82 (Krammer, 2020). Analyses of the B-cell responses to the spike generally focus on the RBD and on cells
83 sorted with RBD baits (Cao et al., 2020; Gaebler et al., 2020; Robbiani et al., 2020; Weisblum et al., 2020).
84 This is also true for B cells and monoclonal antibodies (mAbs) isolated from vaccinated individuals (Wang
85 et al., 2021). However, other epitopes within the spike protein, notably the N-terminal domain (NTD) but
86 also S2, do harbor neutralizing epitopes (Chi et al., 2020; Liu et al., 2020; McCallum et al., 2021; Song et
87 al., 2020). In fact, the NTD is heavily mutated in all three current variants of concern (VOCs, B.1.1.7,
88 B.1.351 and P.1 (Davies et al., 2021; Faria et al., 2021; Tegally et al., 2020)). Here, we studied the unbiased
89 plasmablast response to SARS-CoV-2 mRNA-based vaccination and report the co-dominance of RBD and
90 NTD as B-cell targets on the viral spike protein.

91

Results

The polyclonal antibody response to mRNA vaccination exceeds titers seen in convalescent individuals but is characterized by a high ratio of non-neutralizing antibodies

In late 2020, six adults (**Supplemental Table 1**) who were participating in an ongoing observational study received the mRNA-based SARS-CoV-2 vaccines. Blood from these individuals (V1-V6) was collected at several time points including before vaccination (for 4/6), after the first vaccination and at several time points after the second vaccination. We examined their immune responses to recombinant spike protein and RBD in enzyme-linked immunosorbent assays (ELISA), in comparison to those of 30 COVID-19 survivors (**Figure 1A and B**). The sera from convalescent individuals were selected based on their anti-spike titers (low +: n=8; moderate ++: n=11; and high +++: n=11). Five out of six vaccinees produced anti-spike and anti-RBD responses that were markedly higher than responses observed even in the high titer convalescent group while one vaccinee (V4) produced titers comparable to the high titer group. Notably, the antibody response peaked one week after second vaccine dose, followed by a decline in titers over the following weeks as expected from an antibody response to vaccination. We also measured neutralizing antibody titers using authentic SARS-CoV-2 and found a similar trend with all vaccinees displaying high titers, even though V4 responded with delayed kinetics (**Figure 1C**). Importantly, although at the peak response, the vaccine group mounted neutralization titers that fell in the upper range for the high convalescent group, they did not exceed that group markedly. This finding prompted us to calculate the proportions of spike binding to neutralizing antibodies. For the convalescent group, we found that individuals with lower titers had a higher proportion of binding to neutralizing antibodies than high responding convalescent individuals (**Figure 1D**). When determined at the time of peak response, the vaccinees had the highest proportion of binding to neutralizing antibody titers, indicating an immune response focused on non-neutralizing antibodies or an induction of less potent neutralizing antibodies in general (or both).

mRNA vaccination induces a modest but measurable immune response to seasonal β-coronavirus spike proteins

It has been reported that SARS-CoV-2 infection induces an original antigenic sin-type immune response against human coronaviruses (hCoVs) to which the majority of the human population has pre-existing immunity (Aydillo et al., 2020; Song et al., 2020). Here, we explored whether this phenomenon is also induced by SARS-CoV-2 mRNA vaccination. Antibody titers in four vaccinees against spike protein from α-coronaviruses 229E and NL63 were detectable at the pre-vaccination time point, but did not increase substantially post-vaccination (**Figure 1E-F**; for V5 and V6 no pre-vaccination serum was available). However, titers against the spike proteins of β-coronaviruses OC43 and HKU1 increased substantially in these four vaccinees after vaccination (**Figure 1G-H)**. Thus, vaccination with mRNA SARS-CoV-2 spike also boosts seasonal β-coronaviruses immune responses in a manner reminiscent of that reported for natural infection with SARS-CoV-2.

Plasmablast response to SARS-CoV-2 mRNA vaccination targets both the RBD and the NTD

In order to characterize the B-cell response to vaccination in an unbiased manner, plasmablasts were single-cell sorted from blood specimens obtained from three individuals (V3, V5 and V6) one week after the booster immunization (**Suppl. Figure 1**). All mAbs were generated from single-cell sorted plasmablasts and probed for binding to recombinant SARS-CoV-2 spike protein. Twenty-one (40 mAbs

133 were screened, with 28 being clonally unique) spike-reactive mAbs were isolated from V3, six (82
134 screened, 20 unique) from V5 and fifteen (84 screened, 24 unique) from V6 (**Figure 2A**). Interestingly, only
135 a minority of these antibodies recognized RBD (24% for V3, 47% for V6 and no RBD binders were identified
136 for V5) (**Figure 2B and D**). A substantial number of the isolated mAbs bound to NTD including 14% for V3,
137 33% for V5 and 33% for V6 (**Figure 2C and D**). These data indicate that RBD and NTD are co-dominant in
138 the context of mRNA-induced plasmablast response. The epitopes for the remaining spike binding mAbs,
139 62% for V3, 67% for V5 and 20% for V6, likely bind to epitopes outside of the NTD and RBD.

140 **The majority of isolated mAbs are non-neutralizing**

141 All antibodies were tested for neutralizing activity against the USA-WA1/2020 strain of SARS-CoV-
142 2. Only a minority of the binding antibodies, even those targeting the RBD, showed neutralizing activity
143 (**Figure 2E and F**). For V3, only one (an RBD binder) out of 21 mAbs (5%) displayed neutralizing activity
144 (**Figure 2F**). For V5, a single NTD antibody neutralized authentic SARS-CoV-2 (17%) (**Figure 2F**). The highest
145 frequency of neutralizing antibodies was found in V6 (34%) with one RBD neutralizer and four NTD
146 neutralizers (**Figure 2F**). Interestingly, the highest neutralizing potency was found in mAb PVI.V5-6, an
147 NTD binder followed by PVI.V6-4, an RBD binder.

148 We also tested all antibodies for reactivity to the spike proteins of hCoVs 229E, NL63, HKU1 and
149 OC43. No antibody binding to the spike proteins of α-coronaviruses 229E and NL63 was found but we
150 identified five mAbs (including three from V3, one from V5 and one from V6) that bound to variable
151 degrees to the spike of OC43, which, like SARS-CoV-2, is a β-coronavirus (**Figure 2G**). Three mAbs showed
152 strong binding (PVI.V3-8, PVI.V3-12 and PVI.V6-1), while PVI.V3-17 showed an intermediate binding
153 phenotype and PVI-V5-1 bound very weakly. Three of these mAbs also showed binding to the spike of
154 HKU1, another β-coronavirus. Of these, PVI.V6-1 showed only very weak binding while PVI.3-8 and PVI.3-
155 12 had low minimal binding concentrations (MBCs) indicating higher affinity (**Figure 2H**).

156 **The spike-reactive plasmablast response is dominated by IgG1+ cells and is comprised of a mixture of**
157 **cells with low and high levels of somatic hypermutation (SHM)**

158 Single-cell RNA sequencing (scRNAseq) was performed on bulk sorted plasmablasts from the
159 three vaccinees (V3, V5, V6) to comprehensively examine the transcriptional profile, isotype distribution
160 and somatic hypermutation (SHM) of vaccine-induced plasmablasts. We analyzed 4,584; 3,523 and 4,461
161 single cells from subjects V3, V5, and V6, respectively. We first verified the identity of sequenced cells as
162 plasmablasts through the combined expression of B cell receptors (BCRs) (**Figure 3A**) and that of the
163 canonical transcription as well as other factors essential for plasma cell differentiation, such as *PRDM1*,
164 *XBP1* and *MZB1* (**Figure 3B**). To identify vaccine-responding B cell clones among the analyzed
165 plasmablasts, we used scRNAseq to also analyze gene expression and V(D)J libraries from the sorted
166 plasmablasts and clonally matched the BCR sequences to those from which spike-specific mAbs had been
167 made. Using this method, we recovered 332, 7 and 1384 BCR sequences from the scRNAseq data that are
168 clonally related to the spike-binding mAbs derived from subjects V3, V5 and V6, respectively (**Figure 3C**).
169 It is important to note here that we were not able to recover clonally related sequences for all of the mAbs
170 we cloned and expressed from each of the three vaccinees.

171 We next examined the isotype and IgG subclass distribution among the recovered sequences.
172 IgG1 was by far the most dominant isotype in the three vaccinees (**Figure 3D**). Finally, we assessed the
173 level of somatic hypermutation (SHM) among the mAbs-related sequences from the three subjects. We

174 used the SHM levels observed in human naïve B cells and seasonal influenza virus vaccination-induced
175 plasmablasts that were previously published for comparison (Turner et al., 2020). Spike-reactive
176 plasmablasts from V3 and V6 but not V5 had accumulated SHM at levels that are significantly greater than
177 those observed with naïve B cells (**Figure 3E, left panel**). Strikingly, the SHM among V6 plasmablasts was
178 equivalent to those observed after seasonal influenza virus vaccination (**Figure 3E, left panel**). We
179 reasoned that the high level of SHM among spike-reactive plasmablasts may be derived from those
180 targeting conserved epitopes that are shared with human β-coronaviruses. Indeed, we found that the
181 SHM level among clones that are related to cross-reactive mAbs was significantly higher than their non-
182 cross-reactive counterparts (**Figure 3E, right panel**).

183 **Affinity of variant RBDs for human ACE2**

184 Since we were prepared RBD proteins of viral variants of concern for analysis of antibody binding,
185 we also wanted to assess the affinity of each variant RBD for human ACE2. Using biolayer interferometry
186 (BLI), we measured rates of association and dissociation of the N501Y RBD mutant (B.1.1.7 carries that
187 mutation as its sole RBD mutation), Y453F as found in mink isolates (Larsen et al., 2021), N439K which is
188 found in some European clades (Thomson et al., 2021), a combination of Y453F and N439K, E484K (part
189 of B.1.351 and P.1) as well as for the B.1.351 RBDs for a recombinant version of human ACE2. Almost all
190 single and double mutations in RBD tested increased affinity to human ACE2. Specifically, N501Y and
191 Y453F combined with N439K increased affinity for human ACE2 by 5-fold (**Figure 4, Suppl. Figure 2**). In
192 contrast, E484K on its own decreased affinity by 4-fold. Of note, the B.1.351 RBD affinity for ACE2 was
193 comparable to that of the wild type RBD.

194 **Binding profiles of polyclonal serum and mAbs to RBDs carrying mutations found in viral variants of**
195 **concern**

196 Next, we assessed binding of sera from vaccinated individuals, COVID-19 survivors and mAbs
197 derived from plasmablasts to variant RBDs. Our panel of RBDs includes published mAb escape mutants,
198 RBD mutants detected by the Mount Sinai Hospital's Pathogen Surveillance Program in patients seeking
199 care at the Mount Sinai Health System in NYC as well as mutations found in viral variants of interest and
200 variants of concern (Baum et al., 2020; Greaney et al., 2021; Larsen et al., 2021; Thomson et al., 2021;
201 Weisblum et al., 2020). Serum from convalescent individuals showed strong fluctuations depending on
202 the variant (**Figure 5A**). In general, single mutants E406Q, E484K and F490K exerted the biggest impact on
203 binding. However, complete loss of binding was rare and 2-4-fold reduction in binding was more common.
204 Interestingly, almost all sera bound better to N501Y RBD (B.1.1.7) than to wild type (average 129%
205 compared to wild type). Conversely, the B.1.351 RBD caused on average a 39% reduction in binding. The
206 impact was slightly lower for the P.1 RBD (average 70% binding compared to wild type). For sera from the
207 six vaccinated individuals, however, the highest reduction seen was only two-fold for E406Q, N440K,
208 E484K and F490K (**Figure 5B**). The highest reduction observed for E484K, F484A, B.1.351 and P.1 were
209 also approximately two-fold but this did not apply to all six vaccinees. Some vaccinees maintained binding
210 levels against these RBDs at levels comparable to wild type RBD.

211 RBD binding mAbs were also tested for binding to the same variants. In general, mAbs maintained
212 binding levels within 2-fold of the binding seen with the wild type RBD with some exceptions. In fact, for
213 most mAbs, no impact on binding was observed (**Figure 5C**) with the exception of PVI.V3-9, which lost
214 binding to the RBD carrying F486A. Although there was a negative impact on binding of several mAbs to

215 the B.1.351 variant, binding was almost unaffected by the mutations in the P.1 variant RBD. Only one
216 mAb, PVI.V6-4, showed a drop in binding against P.1.

217 **Escape of an NTD and E484K mutant virus from polyclonal post-vaccination serum is negligible but**
218 **NTD mutations significantly impact the neutralizing activity of NTD binding mAbs**

219 Through the Mount Sinai Hospital's Pathogen Surveillance Program, we had access to the SARS-
220 CoV-2 isolate PV14252 (Clade 20C, Pango lineage B.1) that featured two mutations (W64R, L141Y) and
221 one deletion (Δ142-145) in the NTD as well as the E484K mutation in the RBD (strain, **Figure 5D**). To
222 determine the susceptibility of this virus variant to neutralization by post-vaccination serum, we
223 performed microneutralization assays. Wild type SARS-CoV-2 and PV14252 were tested in parallel with
224 the antiviral drug remdesivir serving as control to ensure that the assay setup for both viruses allowed
225 comparison. The activity of remdesivir on both viruses was comparable. (**Figure 5E**). We found a relatively
226 minor impact when testing polyclonal sera from vaccinees for neutralizing activity (**Figure 5F**). The activity
227 of sera from V2, V5 and V6 slightly increased while the activity for V1, V3 and V4 decreased. Next, we
228 tested the seven neutralizing mAbs that we isolated from plasmablasts. Consistent with their binding
229 profiles in the variant RBD ELISA, the two RBD mAbs neutralized both viruses with comparable efficiency.
230 In fact, the activity of PVI.V3-9 increased slightly (**Figure 5G**). In stark contrast, all five anti-NTD antibodies
231 completely lost neutralizing activity against PV14252 due to mutations present in the NTD of this viral
232 isolate.

233

234 **Discussion**

235 Our knowledge of B-cell responses to SARS-CoV-2 mRNA vaccination remains incomplete. We
236 urgently need information about the nature of polyclonal vaccine-induced responses as well as unbiased,
237 in depth analyses of plasmablast responses. Our data provide important new insights into these responses
238 in comparison with immune responses to natural infection. Indeed, SARS-CoV-2 infection results in a very
239 heterogeneous antibody response to the spike protein in terms of antibody quantity. In contrast, mRNA
240 vaccination appears to induce a high antibody response of relatively homogenous titers. However, we
241 also found that vaccinees generate more non-neutralizing antibodies than COVID-19 survivors resulting in
242 a worse ratio of neutralizing to binding antibodies. These data were already apparent in the early phase
243 clinical trials but remained unrecognized at the time (Walsh et al., 2020). Interestingly, low titer
244 convalescent serum had the highest relative amount of neutralizing antibodies, whereas the proportion
245 of binding antibodies was increased in sera with higher measured antibody titers. The majority of
246 plasmablasts sampled after vaccination do, in fact, produce non-neutralizing antibodies. Future studies
247 are needed to reveal the role of non-neutralizing antibodies in SARS-CoV-2 immune protection. Indeed,
248 antibody functions other than neutralization have been shown to correlate with protection (Bartsch et al.,
249 2021; Gorman et al., 2021; Schäfer et al., 2021). The importance of absolute antibody titers and not ratios
250 is underscored by the fact that post-vaccination neutralization titers were equal to or exceeded the titers
251 found in the high responder convalescent group.

252 Of the four seasonal CoVs are widely circulating in humans but OC43 and HKU1 have higher
253 homology to SARS-CoV-2 spike. Vaccinated individuals mounted a response to spike proteins from β-
254 coronaviruses OC43 and HKU1 but not to α-coronaviruses 229E and NL63. This phenomenon resembles
255 the immune imprinting described in influenza virus immunology and has already been described for
256 natural infection with SARS-CoV-2 (Aydillo et al., 2020; Song et al., 2020). A few of the mAbs isolated in
257 our study also had such cross-reactive phenotype. It remains unclear whether these antibodies, which
258 target epitopes outside of the NTD and RBD, contribute to protection against SARS-CoV-2, OC43 or HKU1
259 infection. However, the cross-reactive epitopes of mAbs that do bind SARS-CoV-2, HKU1 and OC43 spikes
260 could provide the basis for future pan-β-coronavirus vaccines.

261 Another interesting point we noted is the co-dominance of RBD and NTD. Previous analyses of B-
262 cell responses to SARS-CoV-2 mRNA vaccination focused on cells baited by labeled RBD (Wang et al.,
263 2021). We, in contrast, took an unbiased approach to sort and clone plasmablasts in an antigen-agnostic
264 manner. We found similar levels of NTD and RBD binders with many mAbs binding to epitopes outside the
265 RBD and the NTD. In one vaccinee not a single RBD binding mAbs was isolated with the caveats that the
266 overall number of mAbs derived from that individual were low and their polyclonal serum antibody
267 responses included RBD recognition. These data suggest that the NTD, which also harbors neutralizing
268 epitopes, is - at least - as important as the RBD and warrants as much attention. In fact, five out of seven
269 neutralizing antibodies isolated in this study bound to the NTD and only two targeted the RBD. Thus, a re-
270 evaluation of the B cell responses to natural SARS-CoV-2 infection with unbiased approaches is needed to
271 understand if the co-dominance of NTD and RBD is vaccine specific or also seen upon natural infection.
272 Further characterization of the mAbs obtained in this study showed a complete loss of neutralization
273 against an authentic, replication-competent variant virus that harbored extensive changes in the NTD.
274 These observations may explain why a reduction in neutralization against the viral variant of concern
275 B.1.17 is seen in some studies despite the fact the N501Y substitution in the RBD of this variant does not
276 significantly impact binding and neutralizing activity (Emary et al., 2021).

277 We also assessed the impact of different RBD mutations on affinity towards human ACE2.
278 Interestingly, N501Y increased the affinity by five-fold. This increase in receptor binding affinity may
279 contribute to the higher infectivity of B.1.1.7, which carries this mutation in its RBD. In contrast,
280 introduction of E484K reduced the affinity by 4-fold which may explain why virus variants carrying only
281 the E484K mutation have rarely spread efficiently, although viruses carrying E484K have been detected
282 since the fall of 2020 in a handful of patients receiving care at the Mount Sinai Health System and have
283 also been reported in immunocompromised patients (Choi et al., 2020). It is tempting to speculate that
284 the N501Y mutation enables the acquisition of E484K without a fitness loss. In fact, the B.1.351 RBD, which
285 carries N501Y and E484K (as well as N417K) showed binding to hACE2 that was similar to wild type RBD.
286 Recently, B.1.1.7 variant strains carrying E484K, in addition to N501Y, have been isolated in the UK (PHE,
287 2021), providing evidence for the hypothesis that N501Y enables acquisition of mutations in the RBD that
288 may be detrimental to receptor binding. However, recent expansion of B.1.526, a lineage also featuring
289 E484K but without N501Y in New York City, suggests that this fitness loss may be overcome by other, yet
290 uncharacterized, changes in the virus as well (Annavajhala et al., 2021; Lasek-Nesselquist et al., 2021).
291 Interestingly, binding of convalescent sera to the N501Y RBD was also increased, suggesting that changes
292 that increase affinity for the receptor may also increase affinity of a set of antibodies that may mimic the
293 receptor.

294 We also noted that the two neutralizing antibodies against the RBD showed some reduced binding
295 to a mutant RBD carrying the E484K mutation while having similar or even increased neutralizing potency
296 against a variant virus carrying the E484K mutation as the only change in its RBD. The reduced affinity of
297 the E484K variant RBD for hACE2 could render the virus more susceptible to RBD binding mAbs. Thus, an
298 antibody binding to the RBD may just be more effective in interfering with a low affinity as compared to
299 a high affinity RBD-hACE2 interaction. Increased affinity as an escape mechanism for viruses has been
300 described in the past (Hensley et al., 2009; O'Donnell et al., 2012) and the converse mechanism could be
301 at play here.

302 Whether or not the current vaccines will provide effective protection against circulating and
303 emerging viral variants of concern is an important question which has gathered a lot of attention in early
304 2021. Our data indicate that reduction in binding to the E484K and B.1.351 variant RBDs was minor (often
305 only 2-fold) compared to reported reduction in neutralization (which ranges from 6-8 fold to complete
306 loss of neutralization (Cele et al., 2021; Wibmer et al., 2021; Wu et al., 2021)). Although not tested here,
307 it is likely that the reduction in binding to full length spike is even lower, given the many epitopes on the
308 spike other than NTD and RBD. The maintenance of binding to a large degree observed in this study
309 suggests that viral variants will have a minor impact on serological assays which are currently in wide use
310 for medical, scientific and public health reasons. Binding, non-neutralizing antibodies have also been
311 shown to have a protective effect in many viral infections (Asthagiri Arunkumar et al., 2019; Dilillo et al.,
312 2014; Saphire et al., 2018) and may be a factor in the substantial residual protection seen in the Johnson
313 &Johnson and Novavax vaccine trials against B.1.351 in South Africa (Shinde et al., 2021). Production of
314 non-neutralizing antibodies may also play a role in protection by mRNA vaccines after the first dose, as it
315 is substantial and occurs during a time when neutralizing antibody titers are either very low or absent
316 (Baden et al., 2020; Dagan et al., 2021; Polack et al., 2020). Finally, although some antibodies may lose
317 neutralizing activity due to reduced affinity, they do still bind. Furthermore, B cells with these specificities
318 potentially could undergo affinity maturation after exposure to a variant virus or a variant spike-
319 containing vaccine, leading to high affinity antibodies to variant viruses of concern.

320 In summary, we demonstrate that the antibody responses to SARS-CoV-2 mRNA vaccination comprise a
321 large proportion of non-neutralizing antibodies and are co-dominated by NTD and RBD antibodies. The
322 NTD portion of the spike represents, thus, an important vaccine target. Since all viral variants of concern
323 are heavily mutated in this region, these observations warrant further attention to optimize SARS-CoV-2
324 vaccines. Finally, broadly cross-reactive mAbs to β-coronavirus spike proteins are induced after
325 vaccination, and suggest a potential development path for a pan- β-coronavirus vaccine.

326 **Acknowledgements**

327 We would like to thank the study participants for their generosity and willingness to participate in
328 longitudinal COVID19 research studies. None of this work would be possible without their contributions.
329 We are also grateful for Mount Sinai's leadership during the COVID-19 pandemic. We want to especially
330 thank Peter Palese, Carlos Cordon-Cardo, Dennis Charney, David Reich and Kenneth Davis for their
331 support. We would also like to thank Bassem Mohamed and Wooseob Kim for their help with preparing
332 the scRNAseq libraries. This work was partially funded by the NIAID Collaborative Influenza Vaccine
333 Innovation Centers (CIVIC) contract 75N93019C00051, NIAID Center of Excellence for Influenza Research
334 and Surveillance (CEIRS, contract # HHSN272201400008C and HHSN272201400006C), NIAID grants
335 U01AI141990 and U01AI150747, by the generous support of the JPB Foundation and the Open
336 Philanthropy Project (research grant 2020-215611 (5384); and by anonymous donors. J.S.T. was
337 supported by NIAID 5T32CA009547.
338

339 **Conflict of interest statement**

340 The Icahn School of Medicine at Mount Sinai has filed patent applications relating to SARS-CoV-2
341 serological assays and NDV-based SARS-CoV-2 vaccines which list Florian Krammer as co-inventor. Viviana
342 Simon is also listed on the serological assay patent application as co-inventors. Mount Sinai has spun out
343 a company, Kantaro, to market serological tests for SARS-CoV-2. Florian Krammer has consulted for Merck
344 and Pfizer (before 2020), and is currently consulting for Pfizer, Seqirus and Avimex. The Krammer
345 laboratory is also collaborating with Pfizer on animal models of SARS-CoV-2. Ali Ellebedy has consulted for
346 InBios and Fimbrion Therapeutics (before 2021) and is currently a consultant for Mubadala Investment
347 Company. The Ellebedy laboratory received funding under sponsored research agreements that are
348 unrelated to the data presented in the current study from Emergent BioSolutions and from AbbVie.
349

350

351

352

353

354

355

356 **Materials and methods.**

357 **Human subjects and specimen collection**. The study protocols for the collection of clinical specimens from
358 individuals with and without SARS-CoV-2 infection by the Personalized Virology Initiative were reviewed
359 and approved by the Mount Sinai Hospital Institutional Review Board (IRB-16-16772; IRB-16-00791; IRB-
360 20-03374). All participants provided written informed consent prior to collection of specimen and clinical
361 information. All specimens were coded prior to processing and analysis. An overview of the characteristics
362 of the vaccinees as well as the study participants with and without COVID-19 is provided in **Suppl. Table**
363 **1**. The vaccinees received two doses of the Pfizer mRNA vaccine.

364 Whole blood was collected via phlebotomy in serum separator tubes (SST) or ethylenediaminetetraacetic
365 acid (EDTA) tubes. Serum was collected after centrifucation as per manufactuers' instructions. Peripheral
366 blood mononuclear cells (PBMCs) isolation was performed by density gradient centrifugation using
367 SepMate tubes (Stemcell) according to manufactuers' instructions. PBMCs were cryo-preserved and
368 stored in liquid nitrogen until analysis.

369 **Recombinant proteins.** All recombinant proteins were produced using Expi293F cells (Life Technologies).
370 Receptor binding domain (RBD) and spike protein of SARS-CoV-2 (GenBank: MN908947.3) was cloned into
371 a mammalian expression vector, pCAGGS as described earlier (Amanat et al., 2020b; Stadlbauer et al.,
372 2020). RBD mutants were generated in the pCAGGS RBD construct by changing single residues using
373 mutagenesis primers. All proteins were purified after transient transfections with each respective plasmid.
374 Six-hundred million Expi293F cells were transfected using the ExpiFectamine 293 Transfection Kit and
375 purified DNA. Supernatants were collected on day four post transfection, centrifuged at 4,000 g for 20
376 minutes and finally, the supernatant was filtered using a 0.22 um filter. Ni-NTA agarose (Qiagen) was used
377 to purify the protein via gravity flow and proteins were eluted as previously described (Amanat et al.,
378 2020b; Stadlbauer et al., 2020). The buffer was exchanged using Amicon centrifugal units (EMD Millipore)
379 and all recombinant proteins were finally re-suspended in phosphate buffered saline (PBS). Proteins were
380 also run on a sodium dodecyl sulphate (SDS) polyacrylamide gels (5–20% gradient; Bio-Rad) to check for
381 purity (Amanat et al., 2018; Margine et al., 2013). Plasmids to express recombinant spike proteins of 229E,
382 HKU1, NL63 and OC43 were generously provided by Dr. Barney Graham (Pallesen et al., 2017).

383

384 **ELISA**. Ninety-six well plates (Immulon 4 HBX; Thermo Scientific) were coated overnight at 4°C with
385 recombinant proteins at a concentration of 2 ug/ml in PBS (Gibco; Life Technologies) and 50 uls/well. The
386 next day, the coating solution was discarded. One hundred uls per well of 3% non-fat milk prepared in PBS
387 (Life Technologies) containing 0.01% Tween-20 (TPBS; Fisher Scientific) was added to the plates to block
388 the plates for 1 hour at room temperature (RT). All serum dilutions were prepared in 1% non-fat milk
389 prepared in TPBS. All serum samples were diluted 3-fold starting at a dilution of 1:50. After the blocking
390 step, serum dilutions were added to the respective plates for two hours at RT. Next, plates were washed
391 thrice with 250 uls/well of TPBS to remove any residual primary antibody. Secondary antibody solution
392 was prepared in 1% non-fat milk in TPBS as well and 100 uls/well was added to the plates for 1 hour at
393 RT. For human samples, anti-human IgG conjugated to horseradish peroxidase (HRP) was used at a
394 dilution of 1:3000 (Millipore Sigma; catalog #A0293). For mouse samples, anti-mouse IgG conjugated to
395 HRP was used at the same dilution (Rockland antibodies and assays; catalog #610-4302). Specifically, a
396 mouse anti-histidine antibody (Takara; catalog #631212) was used as a positive control to detect proteins
397 with a hexa-histidine tag. Once the secondary incubation was done, plates were again washed thrice with

398 250uls/well of TPBS. Developing solution was made in 0.05M phosphate-citrate buffer at pH 5 using o-
399 phenylenediamine dihydrochloride tablets (Sigma-Aldrich; OPD) at a final concentration of 0.04 mg/ml.
400 One hundred uls/well of developing solution was added to each plate for exactly 10 minutes after which
401 the reaction was halted with addition of 50 uls/well of 3M hydrochloric acid (HCl). Plates were read at an
402 optical density of 490 nanometers using a Synergy 4 (BioTek) plate reader. Eight wells on each plate
403 received no primary antibody (blank wells) and the optical density in those wells was used to assess
404 background. Area under the curve was calculated by deducting the average of blank values plus 3 times
405 standard deviation of the blank values. All data was analyzed in Graphpad Prism 7. This protocol has been
406 described in detail earlier (Bailey et al., 2019; Wohlbold et al., 2015).

407 Purified monoclonal antibodies were used at a concentration of 30 ug/ml and then subsequently diluted
408 3-fold. Purified monoclonal antibodies were only incubated on the coated plates for an hour. The
409 remaining part of the protocol was the same as above (Amanat et al., 2020a; Wohlbold et al., 2016).

410 **Bio-layer Interferometry Binding Experiments**

411 Bio-layer Interferometry (BLI) experiments were performed using the BLItz system (fortéBIO, Pall
412 Corporation). Recombinant human Fc fusion ACE2 (SinoBiological) was immobilized on an anti-human IgG
413 Fc biosensor, and RBDs were then applied to obtain binding affinities. Single-hit concentrations were
414 tested at 5.8 µM for binding. All measurements were repeated in subsequent independent experiments.
415 K_D values were obtained through local fit of the curves by applying a 1:1 binding isotherm model using
416 vendor-supplied software. All experiments were performed in PBS pH 7.4 and at room temperature.

417 **Viruses and cells.** Vero.E6 cells (ATCC #CRL-1586) cells were maintained in culture using Dulbecco's
418 Modified Eagles Medium (DMEM, Gibco) which was supplemented with 10% fetal bovine serum (FBS,
419 Corning) and antibiotics solution containing 10,000 units/mL of penicillin and 10,000 µg/mL of
420 streptomycin (Pen Strep, Gibco)(10). Wild type SARS-CoV-2 (isolate USA-WA1/2020) was grown in cells
421 for 3 days, the supernatant was clarified by centrifugation at 4,000 g for 5 minutes and aliquots were
422 frozen at -80°C for long term use. A primary virus isolate, PV14252, bearing mutations and deletions in
423 the spike was obtained by incubating 200 uls of viral transport media from the nasopharyngeal swab with
424 Vero.E6 cells. The sequence of the passage 2 viral isolate was identic to the sequence obtained directly
425 from the clinical specimen. Sequencing was performed on the Illumina platform as described previously
426 (Gonzalez-Reiche et al., 2020). Both replication competent viruses were used to test serum from study
427 participants and antibodies for neutralization activity.

428 **Neutralization assay.** Twenty-thousand cells in 100 uls per well were seeded on sterile 96-well cell culture
429 plates one day prior to the neutralization assay. In general, cells were used at 90% confluency to perform
430 the assay. All serum samples were heat-inactivated to eliminate any complement activity. Serial dilutions
431 of serum samples were made in 1X minimal essential medium (MEM; Life Technologies) starting at a
432 dilution of 1:20. All work with authentic SARS-CoV-2 (isolate USA-WA1/2020 and PV14252) was done in a
433 biosafety level 3 (BSL3) laboratory following institutional biosafety guidelines and has been described in
434 much greater detail earlier (Amanat et al., 2020b; Amanat et al., 2020c). Six hundred median cell culture
435 infectious doses ($TCID_{50}$s) of authentic virus (USA-WA1/2020 and PV14252) was added to each serum
436 dilution and virus-serum mixture was incubated together for 1 hour inside the biosafety cabinet. Media
437 from the cells was removed and 120 uls of the virus-serum mixture was added onto the cells for 1 hour at
438 37°C. After one hour, the virus-serum mixture was removed and 100 uls of each corresponding dilution
439 was added to every well. In addition, 100uls of 1X MEM was also added to every well. Cells were incubated

440 for 48 hours at 37°C after which the media was removed and 150 uls of 10% formaldehyde (Polysciences)
441 was added to inactivate the virus. For assay control, remdesivir was used against both the wild type virus
442 as well as the patient isolate. After 24 hours, cells were permeabilized and stained using an anti-
443 nucleoprotein antibody 1C7 as discussed in detail earlier (Amanat et al., 2020b; Sun et al., 2020).

444 **Cell sorting and flow cytometry.** Staining for sorting was performed using cryo-preserved PBMCs in 2%
445 FBS and 2 mM ethylenediaminetetraacetic acid (EDTA) in PBS (P2). Cells were stained for 30 min on ice
446 with CD20-Pacific Blue (2H7, 1:400), Zombie Aqua, CD71-FITC (CY1G4, 1:200), IgD-PerCP-Cy5.5 (IA6-2,
447 1:200), CD19-PE (HIB19, 1:200), CD38-PE-Cy7 (HIT2, 1:200), and CD3-Alexa 700 (HIT3a, 1:200), all
448 BioLegend. Cells were washed twice, and single plasmablasts (live singlet $CD19^{+}$ $CD3^{-}$ IgD^{lo} $CD38^{+}$ $CD20^{-}$
449 $CD71^{+}$) were sorted using a FACSAria II into 96-well plates containing 2 µL Lysis Buffer (Clontech)
450 supplemented with 1 U/µL RNase inhibitor (NEB) and immediately frozen on dry ice, or bulk sorted into
451 PBS supplemented with 0.05% BSA and processed for single cell RNAseq.

452

453 **Monoclonal antibody (mAb) generation.** Antibodies were cloned as described previously (Wrammert et
454 al., 2011). Briefly, VH, Vκ, and Vλ genes were amplified by reverse transcription-PCR and nested PCR
455 reactions from singly sorted plasmablasts using primer combinations specific for IgG, IgM/A, Igκ, and Igλ
456 from previously described primer sets (Smith et al., 2009) and then sequenced. To generate recombinant
457 antibodies, restriction sites were incorporated via PCR with primers to the corresponding heavy and light
458 chain V and J genes. The amplified VH, Vκ, and Vλ genes were cloned into IgG1 and Igκ expression vectors,
459 respectively, as described previously (Nachbagauer et al., 2018; Wrammert et al., 2008). Heavy and light
460 chain plasmids were co-transfected into Expi293F cells (Gibco) for expression, and antibody was purified
461 with protein A agarose (Invitrogen).

462 **Single-cell RNAseq library preparation and sequencing.** Bulk-sorted plasmablasts were processed using
463 the following 10× Genomics kits: Chromium Next GEM Single Cell 5' Kit v2 (PN-1000263); Library
464 Construction Kit (PN-1000190); Chromium Next GEM Chip K Single Cell Kit (PN-1000286); Chromium Single
465 Cell Human BCR Amplification Kit (PN- 1000253), and Dual Index Kit TT Set A (PN-1000215). The cDNAs
466 were prepared after GEM generation and barcoding, followed by GEM RT reaction and bead cleanup
467 steps. Purified cDNA was amplified for 10–14 cycles before cleaning with SPRIselect beads. Then, samples
468 were evaluated on a 4200 TapeStation (Agilent) to determine cDNA concentration. B-cell receptor (BCR)
469 target enrichments were performed on full-length cDNA. Gene expression and enriched BCR libraries were
470 prepared as recommended by the Chromium Next GEM Single Cell 5' Reagent Kits v2 (Dual Index) user
471 guide, with appropriate modifications to the PCR cycles based on the calculated cDNA concentration. The
472 cDNA libraries were sequenced on Novaseq S4 (Illumina), targeting a median sequencing depth of 50,000
473 and 5,000 read pairs per cell for gene expression and BCR libraries, respectively.

474 **Single cell RNAseq analysis.** Single-cell RNA sequencing and BCR sequencing data was processed using
475 Cell Ranger v5.0 and the GRCh38-2020 version of the human genome provided by the manufacturer. Total
476 recovered cells by RNA sequencing were V3: 6,608, V5: 5,256, and V6: 6,325 with a mean of 90.64% read
477 mapped to the genome. Count matrices were processed in R (v4.0.2) using the Seurat (v3.2.2) R package
478 (Stuart et al., 2019). Cells were filtered for percentage of mitochondrial genes less than 15% and number
479 features less than 4,000. The three specimen sequencing runs were integrated using log-normalized count
480 values and canonical correlation approach (Stuart et al., 2019) with 2,000 variable features. The resulting
481 single-cell object underwent principal component analysis and the top 30 principal components were used
482 for uniform manifold approximation and projection and identifying neighbors. Clustering was performed
483 using a resolution of 0.6. The integrated RNA sequencing object included 12,568 cells with V3: 4,584, V5:
484 3,523, and V6: 4,461 cells. The filtered contig annotation output of Cell Ranger vdj were loaded into R and

485 processed using the scRepertoire (v1.1.3) R package (Borcherding et al., 2020). Clonotypes were assigned
486 using igraph (v1.2.6) network analysis of components generated from CDR3 sequences greater than or
487 equal to 0.85 normalized Levenshtein distance. Percent of cells expressing genes along the UMAP
488 embedding was visualized using the schex (v1.3.0) R package. For mutation analysis, heavy chains of mAbs
489 and single-cell BCRs first underwent V(D)J gene annotation using IgBLAST (v1.14.0) (Ye et al., 2013) with
490 human reference (release 201931-4) from the international ImMunoGeneTics information system (IMGT)
491 (Giudicelli et al., 2005) and then parsing using Change-O (v0.4.6) (Gupta et al., 2015). Mutation frequency
492 was calculated, as described in (Turner et al., 2020), using the "calcObservedMutations" function from
493 SHazaM (v.1.0.2) (Gupta et al., 2015) and by counting the number of nucleotide mismatches from the
494 germline sequence in the heavy chain variable segment leading up to the complementary-determining
495 region 3 (CDR3), while excluding the first 18 positions that could be error-prone due to the primers used
496 for generating the mAb sequences.

497

498 **Structure visualization.** Structural figures were modeled and rendered in Pymol (The PyMOL Molecular
499 Graphics System, Version 2.4 Schrödinger, LLC).

500

501 **References**

502 Amanat, F., Duehr, J., Huang, C., Paessler, S., Tan, G.S., and Krammer, F. (2020a). Monoclonal Antibodies
503 with Neutralizing Activity and Fc-Effector Functions against the Machupo Virus Glycoprotein. J Virol *94*.
504 Amanat, F., Duehr, J., Oestereich, L., Hastie, K.M., Ollmann Saphire, E., and Krammer, F. (2018).
505 Antibodies to the Glycoprotein GP2 Subunit Cross-React between Old and New World Arenaviruses.
506 mSphere *3*.
507 Amanat, F., Stadlbauer, D., Strohmeier, S., Nguyen, T.H.O., Chromikova, V., McMahon, M., Jiang, K.,
508 Arunkumar, G.A., Jurczyszak, D., Polanco, J.*, et al.* (2020b). A serological assay to detect SARS-CoV-2
509 seroconversion in humans. Nat Med *26*, 1033-1036.
510 Amanat, F., White, K.M., Miorin, L., Strohmeier, S., McMahon, M., Meade, P., Liu, W.C., Albrecht, R.A.,
511 Simon, V., Martinez-Sobrido, L.*, et al.* (2020c). An In Vitro Microneutralization Assay for SARS-CoV-2
512 Serology and Drug Screening. Curr Protoc Microbiol *58*, e108.
513 Annavajhala, M.K., Mohri, H., Zucker, J.E., Sheng, Z., Wang, P., Gomez-Simmonds, A., Ho, D.D., and
514 Uhlemann, A.C. (2021). A Novel SARS-CoV-2 Variant of Concern, B.1.526, Identified in New York.
515 medRxiv.
516 Asthagiri Arunkumar, G., Ioannou, A., Wohlbold, T.J., Meade, P., Aslam, S., Amanat, F., Ayllon, J., García-
517 Sastre, A., and Krammer, F. (2019). Broadly Cross-Reactive, Nonneutralizing Antibodies against Influenza
518 B Virus Hemagglutinin Demonstrate Effector Function-Dependent Protection against Lethal Viral
519 Challenge in Mice. J Virol *93*.
520 Aydillo, T., Rombauts, A., Stadlbauer, D., Aslam, S., Abelenda-Alonso, G., Escalera, A., Amanat, F., Jiang,
521 K., Krammer, F., Carratala, J.*, et al.* (2020). Antibody Immunological Imprinting on COVID-19 Patients.
522 medRxiv, 2020.2010.2014.20212662.
523 Baden, L.R., El Sahly, H.M., Essink, B., Kotloff, K., Frey, S., Novak, R., Diemert, D., Spector, S.A., Rouphael,
524 N., Creech, C.B.*, et al.* (2020). Efficacy and Safety of the mRNA-1273 SARS-CoV-2 Vaccine. N Engl J Med.
525 Bailey, M.J., Broecker, F., Duehr, J., Arumemi, F., Krammer, F., Palese, P., and Tan, G.S. (2019).
526 Antibodies Elicited by an NS1-Based Vaccine Protect Mice against Zika Virus. mBio *10*.
527 Barnes, C.O., West, A.P., Huey-Tubman, K.E., Hoffmann, M.A.G., Sharaf, N.G., Hoffman, P.R., Koranda,
528 N., Gristick, H.B., Gaebler, C., Muecksch, F.*, et al.* (2020). Structures of Human Antibodies Bound to

SARS-CoV-2 Spike Reveal Common Epitopes and Recurrent Features of Antibodies. Cell *182*, 828-842.e816.

Bartsch, Y.C., Fischinger, S., Siddiqui, S.M., Chen, Z., Yu, J., Gebre, M., Atyeo, C., Gorman, M.J., Zhu, A.L., Kang, J.*, et al.* (2021). Discrete SARS-CoV-2 antibody titers track with functional humoral stability. Nat Commun *12*, 1018.

Baum, A., Fulton, B.O., Wloga, E., Copin, R., Pascal, K.E., Russo, V., Giordano, S., Lanza, K., Negron, N., Ni, M.*, et al.* (2020). Antibody cocktail to SARS-CoV-2 spike protein prevents rapid mutational escape seen with individual antibodies. Science *369*, 1014-1018.

Borcherding, N., Bormann, N.L., and Kraus, G. (2020). scRepertoire: An R-based toolkit for single-cell immune receptor analysis. F1000Res *9*, 47.

Cao, Y., Su, B., Guo, X., Sun, W., Deng, Y., Bao, L., Zhu, Q., Zhang, X., Zheng, Y., Geng, C.*, et al.* (2020). Potent Neutralizing Antibodies against SARS-CoV-2 Identified by High-Throughput Single-Cell Sequencing of Convalescent Patients' B Cells. Cell *182*, 73-84.e16.

Cele, S., Gazy, I., Jackson, L., Hwa, S.-H., Tegally, H., Lustig, G., Giandhari, J., Pillay, S., Wilkinson, E., Naidoo, Y.*, et al.* (2021). Escape of SARS-CoV-2 501Y.V2 variants from neutralization by convalescent plasma. medRxiv, 2021.2001.2026.21250224.

Chi, X., Yan, R., Zhang, J., Zhang, G., Zhang, Y., Hao, M., Zhang, Z., Fan, P., Dong, Y., Yang, Y.*, et al.* (2020). A neutralizing human antibody binds to the N-terminal domain of the Spike protein of SARS-CoV-2. Science *369*, 650-655.

Choi, B., Choudhary, M.C., Regan, J., Sparks, J.A., Padera, R.F., Qiu, X., Solomon, I.H., Kuo, H.H., Boucau, J., Bowman, K.*, et al.* (2020). Persistence and Evolution of SARS-CoV-2 in an Immunocompromised Host. N Engl J Med *383*, 2291-2293.

Dagan, N., Barda, N., Kepten, E., Miron, O., Perchik, S., Katz, M.A., Hernán, M.A., Lipsitch, M., Reis, B., and Balicer, R.D. (2021). BNT162b2 mRNA Covid-19 Vaccine in a Nationwide Mass Vaccination Setting. N Engl J Med.

Dan, J.M., Mateus, J., Kato, Y., Hastie, K.M., Yu, E.D., Faliti, C.E., Grifoni, A., Ramirez, S.I., Haupt, S., Frazier, A.*, et al.* (2021). Immunological memory to SARS-CoV-2 assessed for up to 8 months after infection. Science *371*.

Davies, N.G., Abbott, S., Barnard, R.C., Jarvis, C.I., Kucharski, A.J., Munday, J.D., Pearson, C.A.B., Russell, T.W., Tully, D.C., Washburne, A.D.*, et al.* (2021). Estimated transmissibility and impact of SARS-CoV-2 lineage B.1.1.7 in England. Science, eabg3055.

Dilillo, D.J., Tan, G.S., Palese, P., and Ravetch, J.V. (2014). Broadly neutralizing hemagglutinin stalk-specific antibodies require FcγR interactions for protection against influenza virus in vivo. Nat Med.

Emary (2021). https://papers.ssrn.com/sol3/papers.cfm?abstract_id=3779160.

Faria, N.R., Claro, I.M., Candido, D., Franco, L.A.M., Andrade, P.S., Coletti, T.M., Silva, C.A.M., Sales, F.C., Manula, E.R., Aguiar, R.S.*, et al.* (2021). <h1 data-topic-id="586" style="font-size: 1.7511em; margin: 0px 0px 4px; font-family: Helvetica, Arial, sans-serif; width: 999px; line-height: 1.2; overflow-wrap: break-word; color: rgb(34, 34, 34); background-color: rgb(255, 255, 255);">Genomic characterisation of an emergent SARS-CoV-2 lineage in Manaus: preliminary findings (https://virological.org/t/genomic-characterisation-of-an-emergent-sars-cov-2-lineage-in-manaus-preliminary-findings/586).

Gaebler, C., Wang, Z., Lorenzi, J.C.C., Muecksch, F., Finkin, S., Tokuyama, M., Ladinsky, M., Cho, A., Jankovic, M., Schaefer-Babajew, D.*, et al.* (2020). Evolution of Antibody Immunity to SARS-CoV-2. bioRxiv.

Giudicelli, V., Chaume, D., and Lefranc, M.P. (2005). IMGT/GENE-DB: a comprehensive database for human and mouse immunoglobulin and T cell receptor genes. Nucleic Acids Res *33*, D256-261.

Gonzalez-Reiche, A.S., Hernandez, M.M., Sullivan, M.J., Ciferri, B., Alshammary, H., Obla, A., Fabre, S., Kleiner, G., Polanco, J., Khan, Z.*, et al.* (2020). Introductions and early spread of SARS-CoV-2 in the New York City area. Science.

577 Gorman, M.J., Patel, N., Guebre-Xabier, M., Zhu, A., Atyeo, C., Pullen, K.M., Loos, C., Goez-Gazi, Y.,
578 Carrion, R., Tian, J.-H.*, et al.* (2021). Collaboration between the Fab and Fc contribute to maximal
579 protection against SARS-CoV-2 in nonhuman primates following NVX-CoV2373 subunit vaccine with
580 Matrix-M™ vaccination. bioRxiv, 2021.2002.2005.429759.
581 Grandjean, L., Saso, A., Torres, A., Lam, T., Hatcher, J., Thistlethwayte, R., Harris, M., Best, T., Johnson,
582 M., Wagstaffe, H.*, et al.* (2020). Humoral Response Dynamics Following Infection with SARS-CoV-2.
583 medRxiv, 2020.2007.2016.20155663.
584 Greaney, A.J., Starr, T.N., Gilchuk, P., Zost, S.J., Binshtein, E., Loes, A.N., Hilton, S.K., Huddleston, J.,
585 Eguia, R., Crawford, K.H.D.*, et al.* (2021). Complete Mapping of Mutations to the SARS-CoV-2 Spike
586 Receptor-Binding Domain that Escape Antibody Recognition. Cell Host Microbe *29*, 44-57.e49.
587 Gupta, N.T., Vander Heiden, J.A., Uduman, M., Gadala-Maria, D., Yaari, G., and Kleinstein, S.H. (2015).
588 Change-O: a toolkit for analyzing large-scale B cell immunoglobulin repertoire sequencing data.
589 Bioinformatics *31*, 3356-3358.
590 Guthmiller, J.J., Stovicek, O., Wang, J., Changrob, S., Li, L., Halfmann, P., Zheng, N.Y., Utset, H., Stamper,
591 C.T., Dugan, H.L.*, et al.* (2021). SARS-CoV-2 Infection Severity Is Linked to Superior Humoral Immunity
592 against the Spike. mBio *12*.
593 Hensley, S.E., Das, S.R., Bailey, A.L., Schmidt, L.M., Hickman, H.D., Jayaraman, A., Viswanathan, K.,
594 Raman, R., Sasisekharan, R., Bennink, J.R.*, et al.* (2009). Hemagglutinin receptor binding avidity drives
595 influenza A virus antigenic drift. Science *326*, 734-736.
596 Isho, B., Abe, K.T., Zuo, M., Jamal, A.J., Rathod, B., Wang, J.H., Li, Z., Chao, G., Rojas, O.L., Bang, Y.M.*, et*
597 *al.* (2020). Persistence of serum and saliva antibody responses to SARS-CoV-2 spike antigens in COVID-19
598 patients. Sci Immunol *5*.
599 Iyer, A.S., Jones, F.K., Nodoushani, A., Kelly, M., Becker, M., Slater, D., Mills, R., Teng, E., Kamruzzaman,
600 M., Garcia-Beltran, W.F.*, et al.* (2020). Dynamics and significance of the antibody response to SARS-CoV-
601 2 infection. medRxiv.
602 Krammer, F. (2020). SARS-CoV-2 vaccines in development. Nature *586*, 516-527.
603 Lan, J., Ge, J., Yu, J., Shan, S., Zhou, H., Fan, S., Zhang, Q., Shi, X., Wang, Q., Zhang, L.*, et al.* (2020).
604 Structure of the SARS-CoV-2 spike receptor-binding domain bound to the ACE2 receptor. Nature *581*,
605 215-220.
606 Larsen, H.D., Fonager, J., Lomholt, F.K., Dalby, T., Benedetti, G., Kristensen, B., Urth, T.R., Rasmussen, M.,
607 Lassaunière, R., Rasmussen, T.B.*, et al.* (2021). Preliminary report of an outbreak of SARS-CoV-2 in mink
608 and mink farmers associated with community spread, Denmark, June to November 2020. Euro Surveill
609 *26*.
610 Lasek-Nesselquist, E., Lapierre, P., Schneider, E., George, K.S., and Pata, J. (2021). The localized rise of a
611 B.1.526 SARS-CoV-2 variant containing an E484K mutation in New York State. medRxiv,
612 2021.2002.2026.21251868.
613 Letko, M., Marzi, A., and Munster, V. (2020). Functional assessment of cell entry and receptor usage for
614 SARS-CoV-2 and other lineage B betacoronaviruses. Nat Microbiol *5*, 562-569.
615 Liu, L., Wang, P., Nair, M.S., Yu, J., Rapp, M., Wang, Q., Luo, Y., Chan, J.F., Sahi, V., Figueroa, A.*, et al.*
616 (2020). Potent neutralizing antibodies against multiple epitopes on SARS-CoV-2 spike. Nature *584*, 450-
617 456.
618 Margine, I., Palese, P., and Krammer, F. (2013). Expression of functional recombinant hemagglutinin and
619 neuraminidase proteins from the novel H7N9 influenza virus using the baculovirus expression system. J
620 Vis Exp, e51112.
621 McCallum, M., Marco, A., Lempp, F., Tortorici, M.A., Pinto, D., Walls, A.C., Beltramello, M., Chen, A., Liu,
622 Z., Zatta, F.*, et al.* (2021). N-terminal domain antigenic mapping reveals a site of vulnerability for SARS-
623 CoV-2. bioRxiv.

624 Nachbagauer, R., Shore, D., Yang, H., Johnson, S.K., Gabbard, J.D., Tompkins, S.M., Wrammert, J.,
625 Wilson, P.C., Stevens, J., Ahmed, R.*, et al.* (2018). Broadly Reactive Human Monoclonal Antibodies
626 Elicited following Pandemic H1N1 Influenza Virus Exposure Protect Mice against Highly Pathogenic H5N1
627 Challenge. J Virol *92*.
628 O'Donnell, C.D., Vogel, L., Wright, A., Das, S.R., Wrammert, J., Li, G.M., McCausland, M., Zheng, N.Y.,
629 Yewdell, J.W., Ahmed, R.*, et al.* (2012). Antibody pressure by a human monoclonal antibody targeting
630 the 2009 pandemic H1N1 virus hemagglutinin drives the emergence of a virus with increased virulence
631 in mice. mBio *3*.
632 Pallesen, J., Wang, N., Corbett, K.S., Wrapp, D., Kirchdoerfer, R.N., Turner, H.L., Cottrell, C.A., Becker,
633 M.M., Wang, L., Shi, W.*, et al.* (2017). Immunogenicity and structures of a rationally designed prefusion
634 MERS-CoV spike antigen. Proc Natl Acad Sci U S A *114*, E7348-E7357.
635 PHE (2021). Investigation of novel SARS-CoV-2 variant Variant of Concern 202012/01 Technical briefing 5
636 (https://assets.publishing.service.gov.uk/government/uploads/system/uploads/attachment_data/file/9
637 59426/Variant_of_Concern_VOC_202012_01_Technical_Briefing_5.pdf).
638 Polack, F.P., Thomas, S.J., Kitchin, N., Absalon, J., Gurtman, A., Lockhart, S., Perez, J.L., Pérez Marc, G.,
639 Moreira, E.D., Zerbini, C.*, et al.* (2020). Safety and Efficacy of the BNT162b2 mRNA Covid-19 Vaccine. N
640 Engl J Med.
641 Ripperger, T.J., Uhrlaub, J.L., Watanabe, M., Wong, R., Castaneda, Y., Pizzato, H.A., Thompson, M.R.,
642 Bradshaw, C., Weinkauf, C.C., Bime, C.*, et al.* (2020). Orthogonal SARS-CoV-2 Serological Assays Enable
643 Surveillance of Low-Prevalence Communities and Reveal Durable Humoral Immunity. Immunity *53*, 925-
644 933.e924.
645 Robbiani, D.F., Gaebler, C., Muecksch, F., Lorenzi, J.C.C., Wang, Z., Cho, A., Agudelo, M., Barnes, C.O.,
646 Gazumyan, A., Finkin, S.*, et al.* (2020). Convergent antibody responses to SARS-CoV-2 in convalescent
647 individuals. Nature *584*, 437-442.
648 Rodda, L.B., Netland, J., Shehata, L., Pruner, K.B., Morawski, P.A., Thouvenel, C.D., Takehara, K.K.,
649 Eggenberger, J., Hemann, E.A., Waterman, H.R.*, et al.* (2021). Functional SARS-CoV-2-Specific Immune
650 Memory Persists after Mild COVID-19. Cell *184*, 169-183.e117.
651 Saphire, E.O., Schendel, S.L., Fusco, M.L., Gangavarapu, K., Gunn, B.M., Wec, A.Z., Halfmann, P.J.,
652 Brannan, J.M., Herbert, A.S., Qiu, X.*, et al.* (2018). Systematic Analysis of Monoclonal Antibodies against
653 Ebola Virus GP Defines Features that Contribute to Protection. Cell *174*, 938-952.e913.
654 Schäfer, A., Muecksch, F., Lorenzi, J.C.C., Leist, S.R., Cipolla, M., Bournazos, S., Schmidt, F., Maison, R.M.,
655 Gazumyan, A., Martinez, D.R.*, et al.* (2021). Antibody potency, effector function, and combinations in
656 protection and therapy for SARS-CoV-2 infection in vivo. J Exp Med *218*.
657 Seow, J., Graham, C., Merrick, B., Acors, S., Pickering, S., Steel, K.J.A., Hemmings, O., O'Byrne, A.,
658 Kouphou, N., Galao, R.P.*, et al.* (2020). Longitudinal observation and decline of neutralizing antibody
659 responses in the three months following SARS-CoV-2 infection in humans. Nat Microbiol *5*, 1598-1607.
660 Shinde, V., Bhikha, S., Hossain, Z., Archary, M., Bhorat, Q., Fairlie, L., Lalloo, U., Masilela, M.L.S.,
661 Moodley, D., Hanley, S.*, et al.* (2021). Preliminary Efficacy of the NVX-CoV2373 Covid-19 Vaccine Against
662 the B.1.351 Variant. medRxiv, 2021.2002.2025.21252477.
663 Smith, K., Garman, L., Wrammert, J., Zheng, N.Y., Capra, J.D., Ahmed, R., and Wilson, P.C. (2009). Rapid
664 generation of fully human monoclonal antibodies specific to a vaccinating antigen. Nat Protoc *4*, 372-
665 384.
666 Song, G., He, W.T., Callaghan, S., Anzanello, F., Huang, D., Ricketts, J., Torres, J.L., Beutler, N., Peng, L.,
667 Vargas, S.*, et al.* (2020). Cross-reactive serum and memory B cell responses to spike protein in SARS-CoV-
668 2 and endemic coronavirus infection. bioRxiv.
669 Stadlbauer, D., Amanat, F., Chromikova, V., Jiang, K., Strohmeier, S., Arunkumar, G.A., Tan, J., Bhavsar,
670 D., Capuano, C., Kirkpatrick, E.*, et al.* (2020). SARS-CoV-2 Seroconversion in Humans: A Detailed Protocol
671 for a Serological Assay, Antigen Production, and Test Setup. Curr Protoc Microbiol *57*, e100.

672 Stuart, T., Butler, A., Hoffman, P., Hafemeister, C., Papalexi, E., Mauck, W.M., Hao, Y., Stoeckius, M.,
673 Smibert, P., and Satija, R. (2019). Comprehensive Integration of Single-Cell Data. Cell *177*, 1888-
674 1902.e1821.
675 Sun, W., Leist, S.R., McCroskery, S., Liu, Y., Slamanig, S., Oliva, J., Amanat, F., Schafer, A., Dinnon, K.H.,
676 3rd, Garcia-Sastre, A.*, et al.* (2020). Newcastle disease virus (NDV) expressing the spike protein of SARS-
677 CoV-2 as a live virus vaccine candidate. EBioMedicine *62*, 103132.
678 Tegally, H., Wilkinson, E., Giovanetti, M., Iranzadeh, A., Fonseca, V., Giandhari, J., Doolabh, D., Pillay, S.,
679 San, E.J., Msomi, N.*, et al.* (2020). Emergence and rapid spread of a new severe acute respiratory
680 syndrome-related coronavirus 2 (SARS-CoV-2) lineage with multiple spike mutations in South Africa.
681 medRxiv, 2020.2012.2021.20248640.
682 Thomson, E.C., Rosen, L.E., Shepherd, J.G., Spreafico, R., da Silva Filipe, A., Wojcechowskyj, J.A., Davis,
683 C., Piccoli, L., Pascall, D.J., Dillen, J.*, et al.* (2021). Circulating SARS-CoV-2 spike N439K variants maintain
684 fitness while evading antibody-mediated immunity. Cell.
685 Turner, J.S., Zhou, J.Q., Han, J., Schmitz, A.J., Rizk, A.A., Alsoussi, W.B., Lei, T., Amor, M., McIntire, K.M.,
686 Meade, P.*, et al.* (2020). Human germinal centres engage memory and naive B cells after influenza
687 vaccination. Nature *586*, 127-132.
688 Wajnberg, A., Amanat, F., Firpo, A., Altman, D.R., Bailey, M.J., Mansour, M., McMahon, M., Meade, P.,
689 Mendu, D.R., Muellers, K.*, et al.* (2020). Robust neutralizing antibodies to SARS-CoV-2 infection persist
690 for months. Science *370*, 1227-1230.
691 Walsh, E.E., Frenck, R., Falsey, A.R., Kitchin, N., Absalon, J., Gurtman, A., Lockhart, S., Neuzil, K., Mulligan,
692 M.J., Bailey, R.*, et al.* (2020). RNA-Based COVID-19 Vaccine BNT162b2 Selected for a Pivotal Efficacy
693 Study. medRxiv, 2020.2008.2017.20176651.
694 Wang, Z., Schmidt, F., Weisblum, Y., Muecksch, F., Barnes, C.O., Finkin, S., Schaefer-Babajew, D., Cipolla,
695 M., Gaebler, C., Lieberman, J.A.*, et al.* (2021). mRNA vaccine-elicited antibodies to SARS-CoV-2 and
696 circulating variants. Nature.
697 Weisblum, Y., Schmidt, F., Zhang, F., DaSilva, J., Poston, D., Lorenzi, J.C., Muecksch, F., Rutkowska, M.,
698 Hoffmann, H.H., Michailidis, E.*, et al.* (2020). Escape from neutralizing antibodies by SARS-CoV-2 spike
699 protein variants. Elife *9*.
700 Wibmer, C.K., Ayres, F., Hermanus, T., Madzivhandila, M., Kgagudi, P., Lambson, B.E., Vermeulen, M.,
701 van den Berg, K., Rossouw, T., Boswell, M.*, et al.* (2021). SARS-CoV-2 501Y.V2 escapes neutralization by
702 South African COVID-19 donor plasma. bioRxiv, 2021.2001.2018.427166.
703 Wilson, P., Stamper, C., Dugan, H., Li, L., Asby, N., Halfmann, P., Guthmiller, J., Zheng, N.Y., Huang, M.,
704 Stovicek, O.*, et al.* (2020). Distinct B cell subsets give rise to antigen-specific antibody responses against
705 SARS-CoV-2. Res Sq.
706 Wohlbold, T.J., Chromikova, V., Tan, G.S., Meade, P., Amanat, F., Comella, P., Hirsh, A., and Krammer, F.
707 (2016). Hemagglutinin Stalk- and Neuraminidase-Specific Monoclonal Antibodies Protect against Lethal
708 H10N8 Influenza Virus Infection in Mice. J Virol *90*, 851-861.
709 Wohlbold, T.J., Nachbagauer, R., Xu, H., Tan, G.S., Hirsh, A., Brokstad, K.A., Cox, R.J., Palese, P., and
710 Krammer, F. (2015). Vaccination with adjuvanted recombinant neuraminidase induces broad
711 heterologous, but not heterosubtypic, cross-protection against influenza virus infection in mice. mBio *6*,
712 e02556.
713 Wrammert, J., Koutsonanos, D., Li, G.M., Edupuganti, S., Sui, J., Morrissey, M., McCausland, M.,
714 Skountzou, I., Hornig, M., Lipkin, W.I.*, et al.* (2011). Broadly cross-reactive antibodies dominate the
715 human B cell response against 2009 pandemic H1N1 influenza virus infection. J Exp Med *208*, 181-193.
716 Wrammert, J., Smith, K., Miller, J., Langley, W.A., Kokko, K., Larsen, C., Zheng, N.Y., Mays, I., Garman, L.,
717 Helms, C.*, et al.* (2008). Rapid cloning of high-affinity human monoclonal antibodies against influenza
718 virus. Nature *453*, 667-671.

719 Wrapp, D., Wang, N., Corbett, K.S., Goldsmith, J.A., Hsieh, C.L., Abiona, O., Graham, B.S., and McLellan,
720 J.S. (2020). Cryo-EM structure of the 2019-nCoV spike in the prefusion conformation. Science.
721 Wu, K., Werner, A.P., Moliva, J.I., Koch, M., Choi, A., Stewart-Jones, G.B.E., Bennett, H., Boyoglu-Barnum,
722 S., Shi, W., Graham, B.S.*, et al.* (2021). mRNA-1273 vaccine induces neutralizing antibodies against spike
723 mutants from global SARS-CoV-2 variants. bioRxiv, 2021.2001.2025.427948.
724 Ye, J., Ma, N., Madden, T.L., and Ostell, J.M. (2013). IgBLAST: an immunoglobulin variable domain
725 sequence analysis tool. Nucleic Acids Res *41*, W34-40.

726

727 **Figure Legends**

728 **Figure 1: Antibody responses in individuals vaccinated with mRNA-based SARS-CoV-2 vaccines.**
729 Antibody responses of convalescent individuals and vaccinees to full length spike protein (**A**) and RBD (**B**)
730 as measured by ELISA and neutralizing activity of the sera of the same individuals in a microneutralization
731 assay against authentic SARS-CoV-2 (**C)**. Convalescent individuals were grouped based on their antibody
732 response to spike protein into +, ++, and +++. **D** shows ratios between binding and neutralizing antibody
733 levels in vaccinees and convalescent individuals. Higher ratios indicate a bias towards non-neutralizing
734 antibodies. **E, F, G and H** show antibody responses against α-coronavirus 229E and NL63 and β-coronavirus
735 OC43 and HKU1 spike proteins over time.

736

737 **Figure 2. Characterization of mAbs derived from vaccine plasmablasts**. Binding of plasmablasts derived
738 from three vaccinees (V3, V5 and V6) against full length spike (**A**), RBD (**B**) and NTD (**C**). D shows the
739 percentages of the respective antibodies per subject. **E** shows neutralizing activity of the mABs against
740 authentic SARS-CoV-2 and the proportion of neutralizing antibodies per subject is shown in F. **G and H**
741 show reactivity of mAbs to spike protein of human β-coronaviruses OC43 and HKU1.

742

743 **Figure 3. Characterization of bulk sorted plasmablasts via single-cell RNA sequencing. (A)** Uniform
744 manifold approximation and projection (UMAP) of scRNAseq from bulk plasmablast with recovered BCR
745 sequences (purple) or unrecovered (grey). **(B)** UMAP overlay of percent of cellular population expressing
746 *MZB1*, *PRDM1*, and *XPB1*. Hexbin equals 80 individual cells. (**C**) UMAP overlay of BCR sequences with
747 confirmed spike binding activity. (**D**) Proportional composition of heavy chains genes in the spike binding
748 sequences broken down by sample. **(E)** Comparison of nucleotide-level mutation frequency in
749 immunoglobulin heavy chain variable (IGHV) genes between plasmablasts clonally related to spike binding
750 mAbs from SARS-CoV-2 vaccinees, plasmablasts sorted from PBMCs one week after seasonal influenza
751 vaccination and found in vaccine-responding B cell clones, and naïve B cells found in blood of an influenza
752 vaccinee (left panel); and between plasmablasts from SARS-CoV-2 vaccinees found to be clonally related
753 to spike-binding mAbs that were, respectively, cross-reactive and non-cross-reactive to human β-
754 coronaviruses spike proteins (right panel).

755

756 **Figure 4. Mapping of the amino-acid substitutions and deletions onto the structure of the SARS-CoV-2**
757 **spike glycoprotein.** Mutations of the three major variants of concern B.1.17, B.1.315 and P.1 show in the
758 table on the left are mapped onto the structure of the spike glycoprotein (model generated by

759 superposition of PDB 6M0j and 7C2L (Chi et al., 2020; Lan et al., 2020)). One RBD in the up conformation
760 (red) is bound with ACE2 receptor (pink). NTD is colored blue and the various amino-acid substitutions are
761 shown as yellow spheres. One spike protomer is shown in bold colors while the other two are colored
762 white. BLI- measured binding affinities of the RBD mutants to ACE2, as well as the calculated fold change,
763 are shown in the table on the right.

764

765 **Figure 5. Binding and neutralization of SARS-CoV-2 variants.** Binding of serum samples from convalescent
766 individuals, vaccinees and vaccine derived mAbs to a panel of RBD mutants is shown in **A, B and C**
767 respectively. The red line in A indicates the average reduction. Dotted lines in A and B indicate 100%, the
768 line with smaller dots in C indicated reactivity of the anti-his coating control. **D** shows the spike mutations
769 of virus isolate PVI14252 modelled on a co-crystal structure of the SARS-CoV-2 spike protein with ACE2
770 (model generated by superposition of PDB 6M0j and 7C2L (Chi et al., 2020; Lan et al., 2020)). **E** shows the
771 inhibitory effect of remdesivir on growth of wild type SARS-CoV-2 and PVI14252. Remdesivir was used as
772 control here to show that both viruses when run side by side in a neutralization assay are inhibited to a
773 similar extent. **F and G** show the inhibitory effect of vaccine serum and vaccine derived neutralizing
774 antibodies on both wild type SARS-CoV-2 and PV14252. Of note, these assays were performed side by side
775 but by different operators and on a different Vero cell clone as the neutralization assays shown in Figure
776 2.

777 **Supplemental Table 1**

Vaccinees	**Spike IgG response**	**Sex**	**Age group (yrs)**	**Specimen tested**
V1	Strong positive	F	>60	several longtiudinal time points
V2	Strong positive	M	30-40	several longtiudinal time points
V3	Strong positive	F	50-60	several longtiudinal time points
V4	Strong positive	M	>60	several longtiudinal time points
V5	Strong positive	F	40-50	several longtiudinal time points
V6	Strong positive	F	30-40	several longtiudinal time points
Seronegative, post pandemic		**Sex**	**Age group (yrs)**	**Days from last negative serology test**
N1	Negative	F	40-50	23
N2	Negative	F	20-29	24
N3	Negative	F	20-29	23
N4	Negative	F	30-35	22

Seropositive, natural infection		Sex	Age group (yrs)	Days post onset of COVID 19 symptoms
P1	Weak positive	M	20-29	260
P2	Weak positive	M	50-59	no data available
P3	Weak positive	F	30-39	111
P4	Weak positive	F	30-39	221
P5	Weak positive	F	30-39	254
P6	Weak positive	F	20-29	247
P7	Weak positive	M	30-39	220
P8	Weak positive	F	20-29	Asymptomatic
P9	Moderate positive	M	30-39	no data available
P10	Moderate positive	F	30-39	197
P11	Moderate positive	F	50-59	Asymptomatic
P12	Moderate positive	F	30-39	Asymptomatic
P13	Moderate positive	M	30-39	234
P14	Moderate positive	F	20-29	273
P15	Moderate positive	M	30-39	Asymptomatic
P16	Moderate positive	F	20-29	258
P17	Moderate positive	F	20-29	246
P18	Moderate positive	M	20-29	Asymptomatic
P19	Moderate positive	F	50-59	204
P20	Strong positive	F	50-59	no data available
P21	Strong positive	F	30-39	245
P22	Strong positive	M	NA	170
P23	Strong positive	F	>60	Asymptomatic
P24	Strong positive	F	40-49	no data available
P25	Strong positive	F	50-59	191
P26	Strong positive	F	30-39	no data available
P27	Strong positive	F	50-59	113
P28	Strong positive	M	>60	Asymptomatic
P29	Strong positive	M	18-19	218
P30	Strong positive	M	50-59	219

778

779 **Supplementary Figure 1**. **Gating strategy for sorting plasmablasts from total PBMCs isolated one week**
780 **after second immunization.**

781

782 **Supplementary Figure 2. Representative Biolayer Interferometry binding isotherms from two**
783 **independent experiments. The raw data are show in pink and the Langmuir 1:1 kinetics fit is show in**
784 **black.**

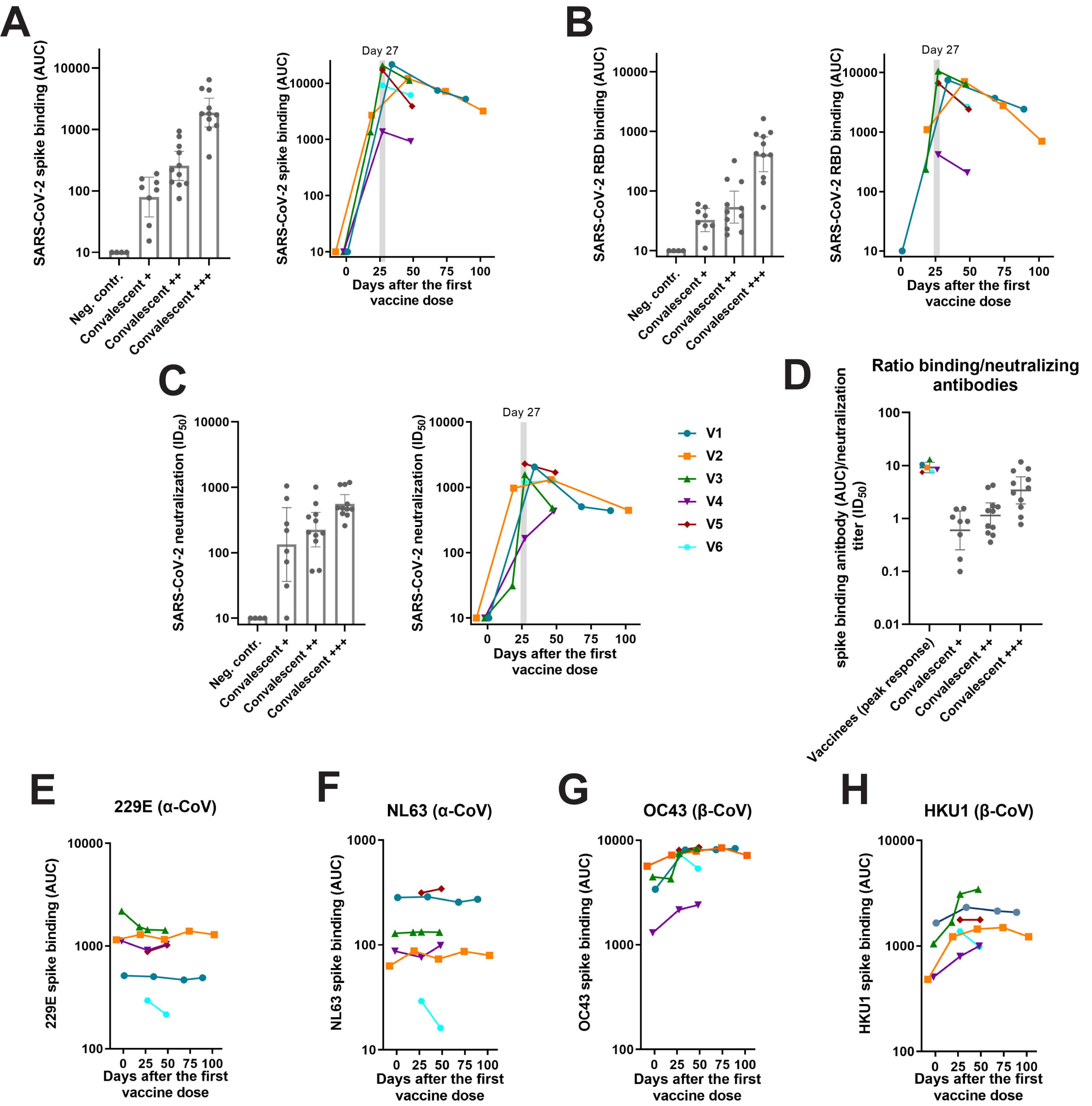
A
SARS-CoV-2 spike binding (AUC)
10000
1000
100
10
Neg. contr.
Convalescent +
Convalescent ++
Convalescent +++
Day 27
Days after the first vaccine dose
B
SARS-CoV-2 RBD binding (AUC)
C
SARS-CoV-2 neutralization (ID50)
V1
V2
V3
V4
V5
V6
D
Ratio binding/neutralizing antibodies
spike binding anitbody (AUC)/neutralization titer (ID50)
100
10
1
0.1
0.01
Vaccinees (peak response)
E
229E (α-CoV)
229E spike binding (AUC)
F
NL63 (α-CoV)
NL63 spike binding (AUC)
G
OC43 (β-CoV)
OC43 spike binding (AUC)
H
HKU1 (β-CoV)
HKU1 spike binding (AUC)
0 25 50 75 100

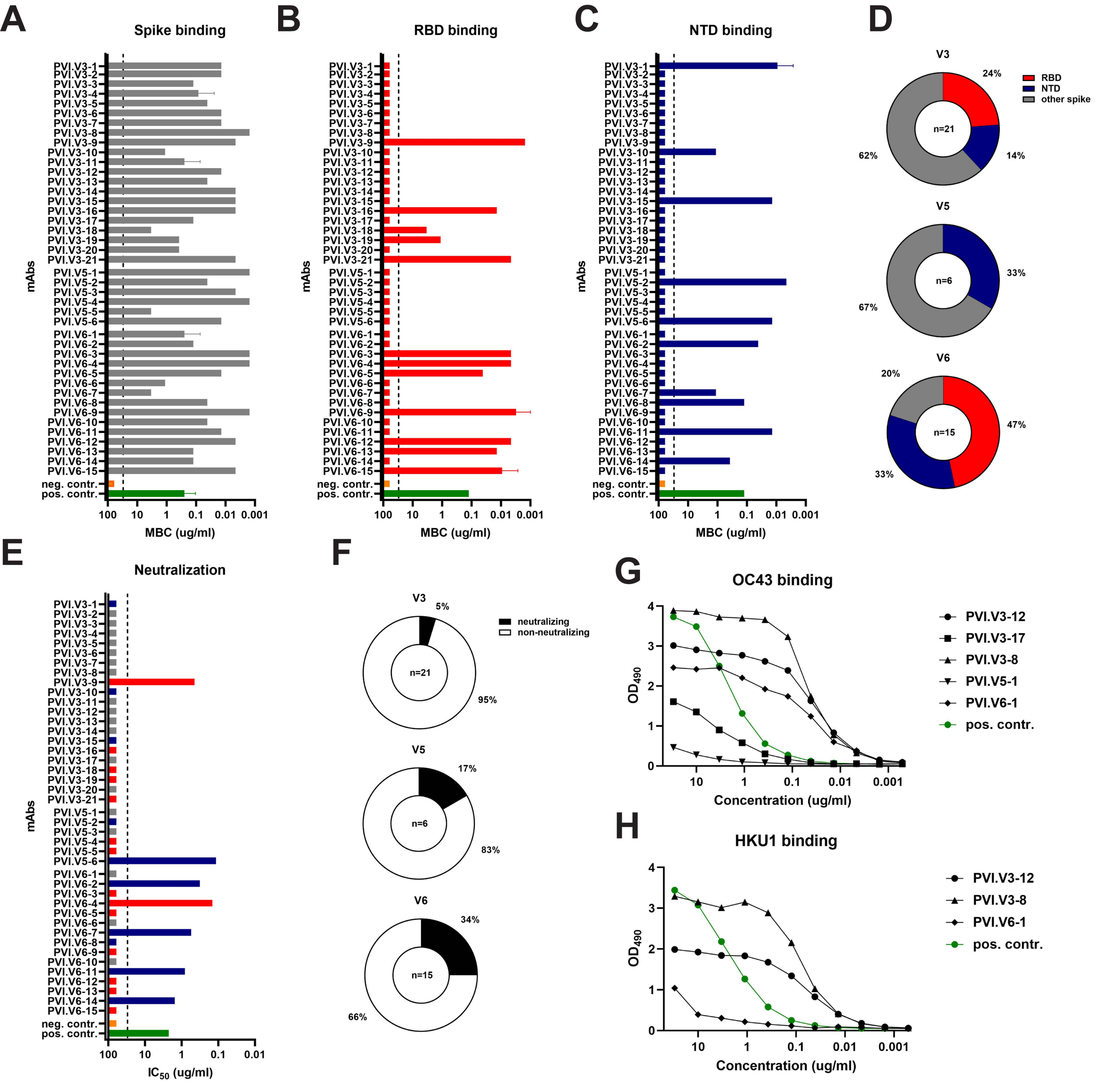
A
Spike binding
mAbs
PVI.V3-1
PVI.V3-2
PVI.V3-3
PVI.V3-4
PVI.V3-5
PVI.V3-6
PVI.V3-7
PVI.V3-8
PVI.V3-9
PVI.V3-10
PVI.V3-11
PVI.V3-12
PVI.V3-13
PVI.V3-14
PVI.V3-15
PVI.V3-16
PVI.V3-17
PVI.V3-18
PVI.V3-19
PVI.V3-20
PVI.V3-21
PVI.V5-1
PVI.V5-2
PVI.V5-3
PVI.V5-4
PVI.V5-5
PVI.V5-6
PVI.V6-1
PVI.V6-2
PVI.V6-3
PVI.V6-4
PVI.V6-5
PVI.V6-6
PVI.V6-7
PVI.V6-8
PVI.V6-9
PVI.V6-10
PVI.V6-11
PVI.V6-12
PVI.V6-13
PVI.V6-14
PVI.V6-15
neg. contr.
pos. contr.
100 10 1 0.1 0.01 0.001
MBC (ug/ml)
B
RBD binding
C
NTD binding
D
V3
24%
14%
62%
n=21
RBD
NTD
other spike
V5
33%
67%
n=6
V6
20%
47%
33%
n=15
E
Neutralization
IC50 (ug/ml)
F
V3
5%
95%
n=21
neutralizing
non-neutralizing
V5
17%
83%
n=6
V6
34%
66%
n=15
G
OC43 binding
OD490
Concentration (ug/ml)
PVI.V3-12
PVI.V3-17
PVI.V3-8
PVI.V5-1
PVI.V6-1
pos. contr.
H
HKU1 binding
PVI.V3-12
PVI.V3-8
PVI.V6-1
pos. contr.

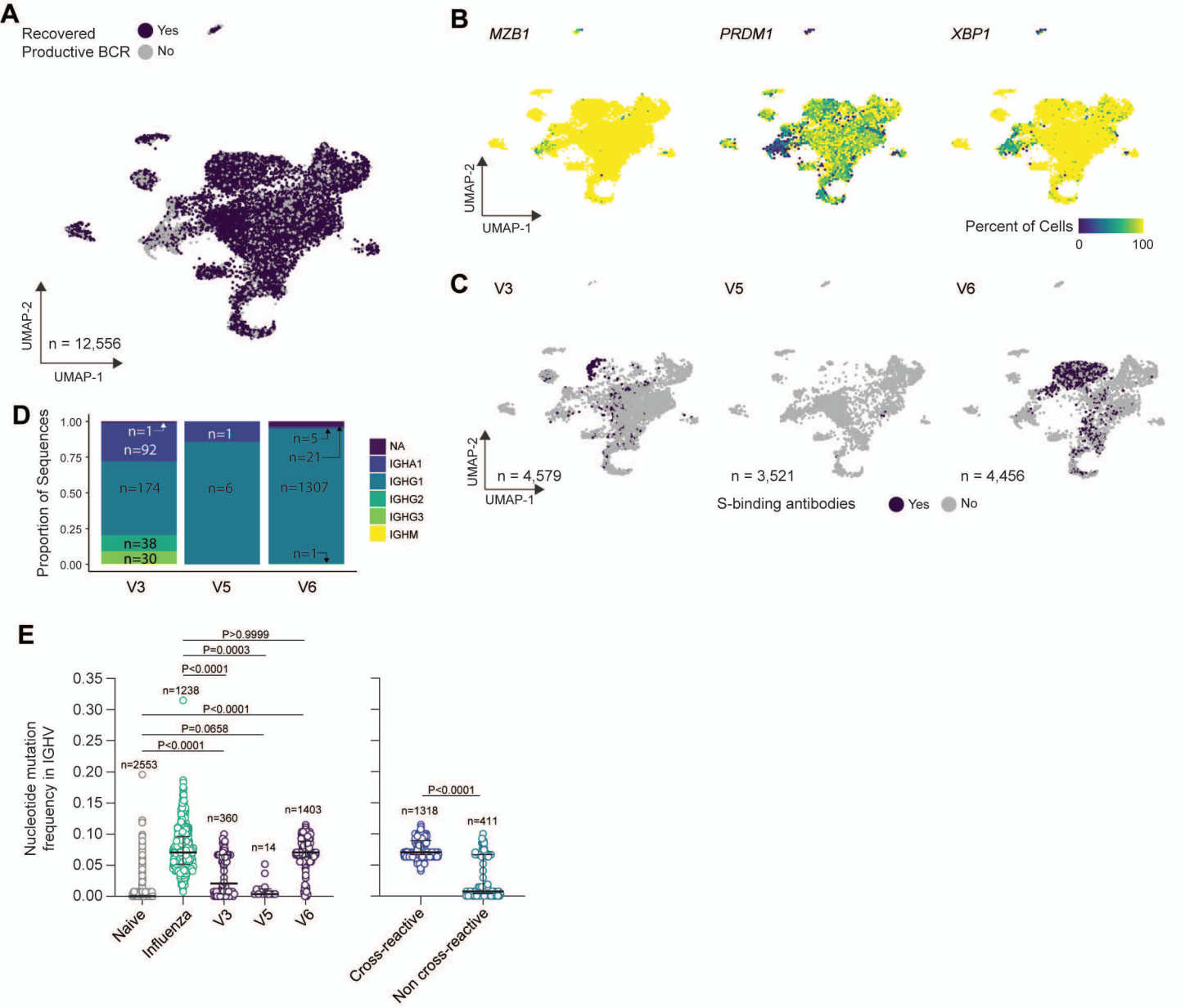
A
Recovered Productive BCR
Yes
No
UMAP-2
UMAP-1
n = 12,556
B
MZB1
PRDM1
XBP1
UMAP-2
UMAP-1
Percent of Cells
0
100
C
V3
V5
V6
UMAP-2
UMAP-1
n = 4,579
n = 3,521
n = 4,456
S-binding antibodies
Yes
No
D
Proportion of Sequences
1.00
0.75
0.50
0.25
0.00
n=1
n=92
n=174
n=38
n=30
n=1
n=6
n=5
n=21
n=1307
n=1
NA
IGHA1
IGHG1
IGHG2
IGHG3
IGHM
V3
V5
V6
E
Nucleotide mutation frequency in IGHV
0.35
0.30
0.25
0.20
0.15
0.10
0.05
0.00
P>0.9999
P=0.0003
P<0.0001
n=1238
P<0.0001
P=0.0658
P<0.0001
n=2553
n=360
n=14
n=1403
P<0.0001
n=1318
n=411
Naive
Influenza
V3
V5
V6
Cross-reactive
Non cross-reactive

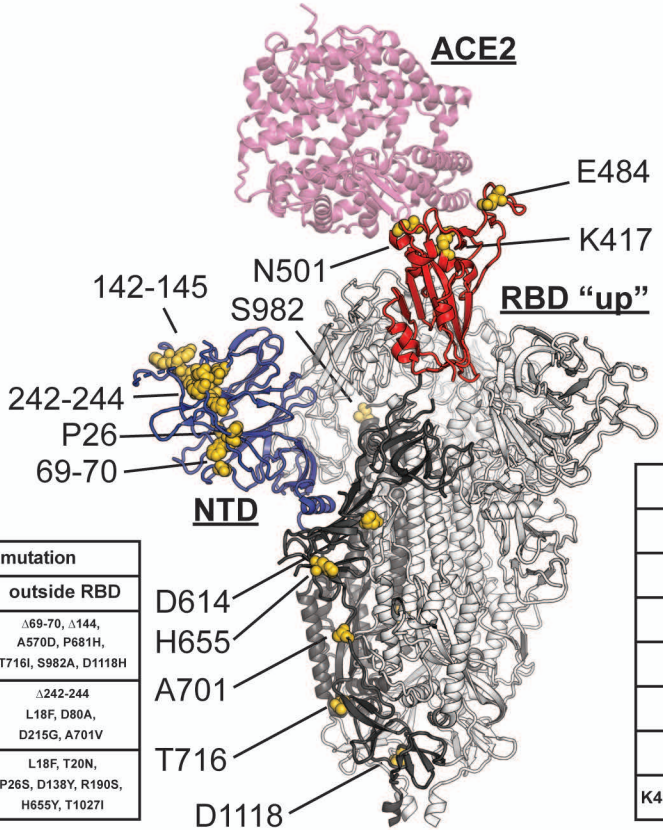

	spike mutation	
variant	RBD	outside RBD
B.1.1.7	N501Y	Δ69-70, Δ144, A570D, P681H, T716I, S982A, D1118H
B.1.351	K417N, E484K, N501Y	Δ242-244 L18F, D80A, D215G, A701V
P.1	K417T, E484K, N501Y	L18F, T20N, P26S, D138Y, R190S, H655Y, T1027I

RBD variant	K_D (nM)	Fold change
wild-type	35.4±5.6	1
N501Y	7.0±1.1	0.2
Y453F	29.9±18.1	0.8
N439K	15.7±3.8	0.4
Y453F/N439K	7.2±0.1	0.2
E484K	138.3±30.9	4
K417N/E484K/N501Y	34.0±4.6	1

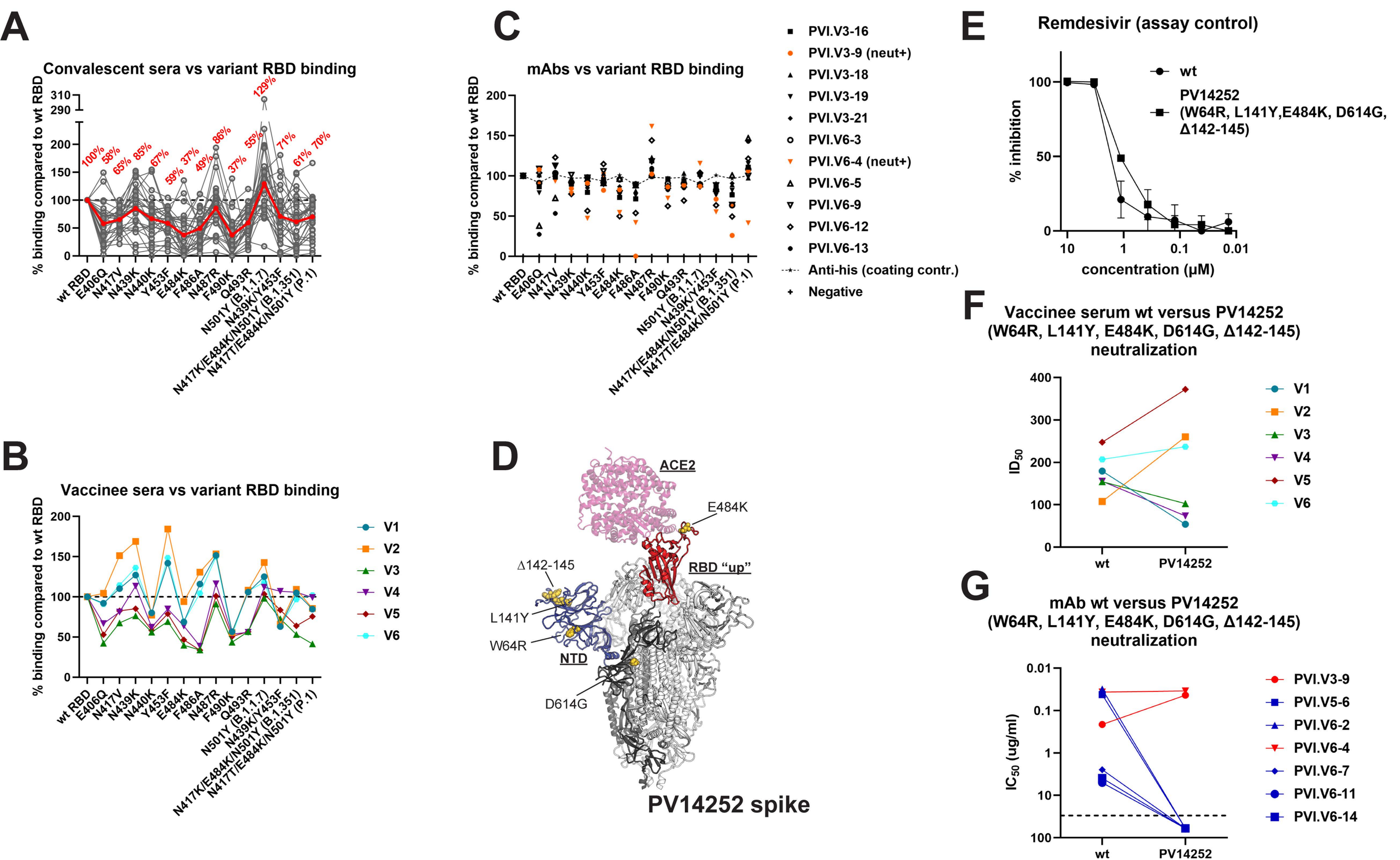
A
Convalescent sera vs variant RBD binding
% binding compared to wt RBD
100%
58%
65%
85%
67%
59%
37%
49%
86%
37%
55%
129%
71%
61%
70%
wt RBD
E406Q
N417V
N439K
N440K
Y453F
E484K
F486A
N487R
F490K
Q493R
N501Y (B.1.1.7)
N439K/Y453F
N501Y (B.1.351)
N417K/E484K/N501Y (P.1)
N417T/E484K/N501Y (P.1)
B
Vaccinee sera vs variant RBD binding
% binding compared to wt RBD
V1
V2
V3
V4
V5
V6
C
mAbs vs variant RBD binding
% binding compared to wt RBD
PVI.V3-16
PVI.V3-9 (neut+)
PVI.V3-18
PVI.V3-19
PVI.V3-21
PVI.V6-3
PVI.V6-4 (neut+)
PVI.V6-5
PVI.V6-9
PVI.V6-12
PVI.V6-13
Anti-his (coating contr.)
Negative
D
ACE2
E484K
Δ142-145
RBD "up"
L141Y
W64R
NTD
D614G
PV14252 spike
E
Remdesivir (assay control)
% inhibition
wt
PV14252
(W64R, L141Y,E484K, D614G,
Δ142-145)
concentration (μM)
F
Vaccinee serum wt versus PV14252
(W64R, L141Y, E484K, D614G, Δ142-145)
neutralization
ID50
V1
V2
V3
V4
V5
V6
G
mAb wt versus PV14252
(W64R, L141Y, E484K, D614G, Δ142-145)
neutralization
IC50 (ug/ml)
PVI.V3-9
PVI.V5-6
PVI.V6-2
PVI.V6-4
PVI.V6-7
PVI.V6-11
PVI.V6-14

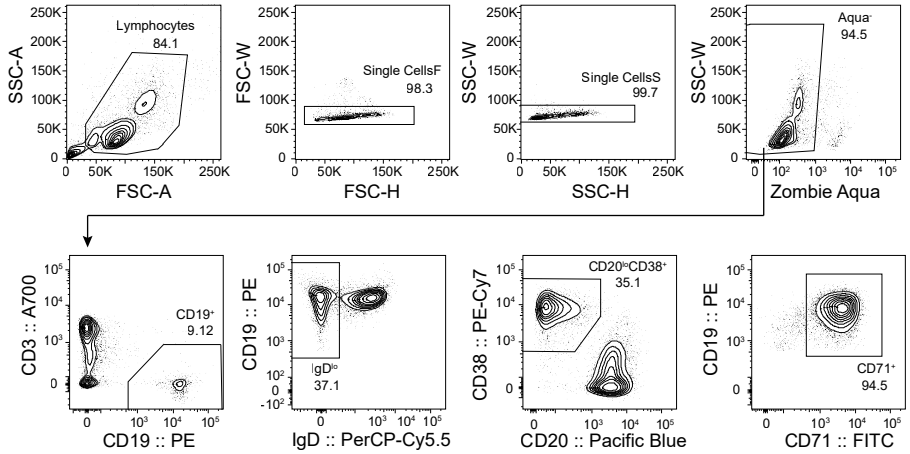
Lymphocytes
84.1
SSC-A
FSC-A
Single CellsF
98.3
FSC-W
FSC-H
Single CellsS
99.7
SSC-W
SSC-H
Aqua-
94.5
SSC-W
Zombie Aqua
CD19+
9.12
CD3 :: A700
CD19 :: PE
IgD-
37.1
CD19 :: PE
IgD :: PerCP-Cy5.5
CD20-CD38+
35.1
CD38 :: PE-Cy7
CD20 :: Pacific Blue
CD71+
94.5
CD19 :: PE
CD71 :: FITC

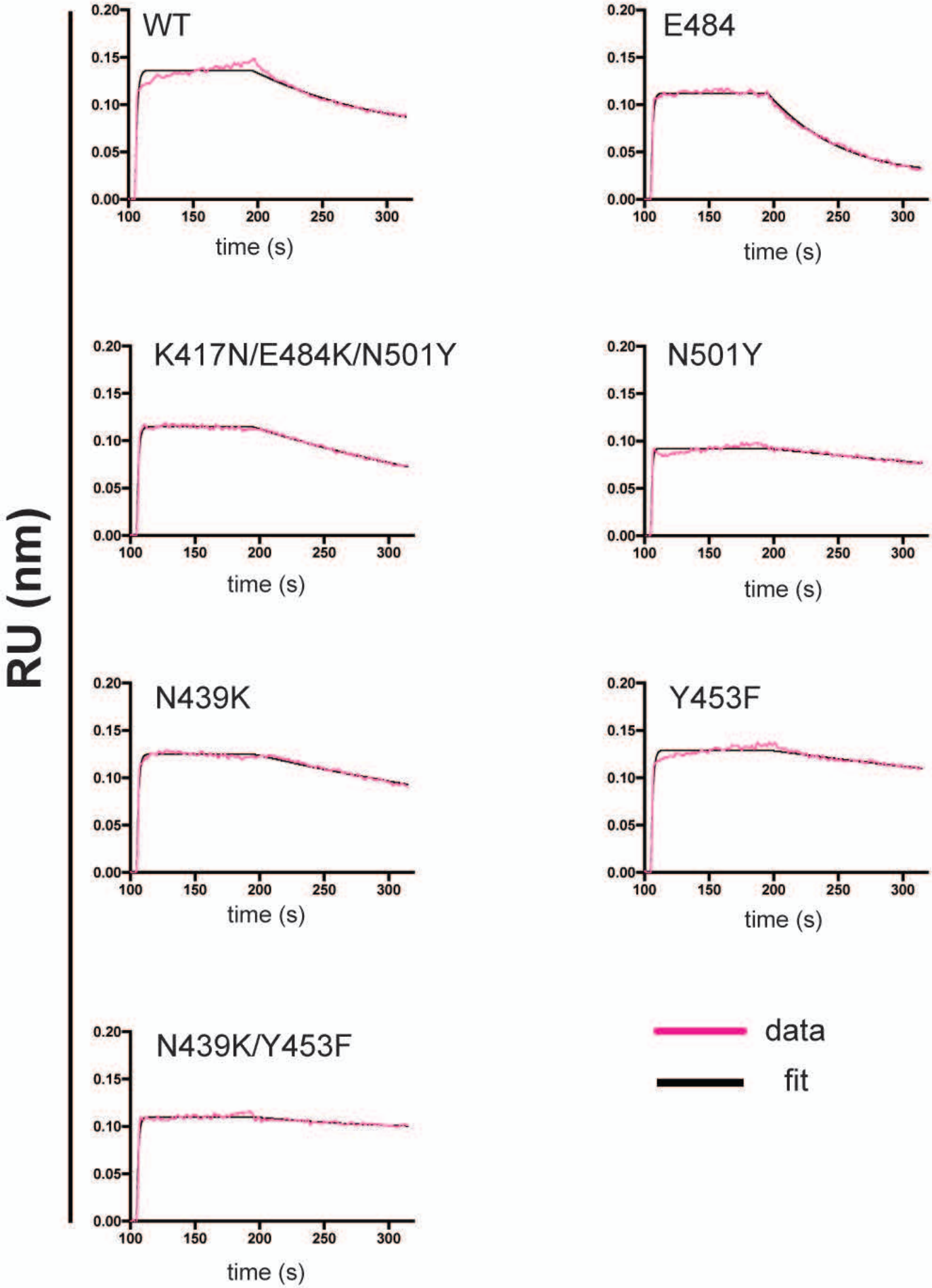
RU (nm)
WT
E484
K417N/E484K/N501Y
N501Y
N439K
Y453F
N439K/Y453F
0.20
0.15
0.10
0.05
0.00
100
150
200
250
300
time (s)
data
fit